Structural Engineering and Mechanics, *Vol. 74, No. 5 (2020) 679-698*
DOI: https://doi.org/10.12989/sem.2020.74.5.679

Meshless Local Petrov-Galerkin (MLPG) method for dynamic analysis of non-symmetric nanocomposite cylindrical shell

Yaser Sadeghi Ferezghi*[1], Mohamadreza Sohrabi[1a] and Seyed Mojtaba Mosavi Nezhad[2b]

[1]*Department of Civil Engineering, Faculty of Engineering, University of Sistan and Baluchestan, Zahedan, Iran*
[2]*Department of Civil Engineering, Faculty of Engineering, University of Birjand, Birjand, Iran*

(Received June 29, 2017, Revised October 5, 2017, Accepted November 27, 2019)

Abstract. In this paper, the meshless local Petrov-Galerkin (MLPG) method is developed for dynamic analysis of non-symmetric nanocomposite cylindrical shell equations of elastic wave motion with nonlinear grading patterns under shock loading. The mechanical properties of the nanocomposite cylinder are obtained based on a micro-mechanical model. In this study, four kinds of grading patterns are assumed for carbon nanotube mechanical properties. The displacements can be approximated using shape function so, the multiquadrics (MQ) Radial Basis Functions (RBF) are used as the shape function. In order to discretize the derived equations in time domains, the Newmark time approximation scheme with suitable time step is used. To demonstrate the accuracy of the present method for dynamic analysis, at the first a problem verifies with analytical solution and then the present method compares with the finite element method (FEM), finally, the present method verifies by using the element free Galerkin (EFG) method. The comparison shows the high capacity and accuracy of the present method in the dynamic analysis of cylindrical shells. The capability of the present method to dynamic analysis of non-symmetric nanocomposite cylindrical shell is demonstrated by dynamic analysis of the cylinder with different kinds of grading patterns and angle of nanocomposite reinforcements. The present method shows high accuracy, efficiency and capability to dynamic analysis of non-symmetric nanocomposite cylindrical shell, which it furnishes a ground for a more flexible design.

Keywords: MLPG; cylindrical shell; nanocomposite; radial basis functions; dynamic analysis; shock loading

1. Introduction

Nanocomposite materials are widely used in light weight structures also to reinforce the cylindrical shell, because these materials have some remarkable properties like as high strength, high stiffness, high aspect ratio and with very low density structures. From engineering perspective, one of the most important problems is dynamic analysis of cylindrical shell of carbon nanotubes reinforced composites.

In the recent years, some researches have been investigated in structures made of nanocomposite materials. A review of carbon nanotubes (2011), Molecular dynamics study of the stress–strain behavior (2007)-(2011), Dynamic analysis of functionally graded nanocomposite (2012) and nonlinear analysis of functionally graded nanocomposite (2013) can be listed as some of previous works. Also some different numerical methods can be possible for the analysis of plates and shells such as DSC, HDQ, and DQ. New exact solutions for vibration of thin circular cylindrical shells with intermediate ring supports, based on the Goldenveizer–Novozhilov shell theory was presented by Xiang *et al*. (2002). Civalek (2008) developed. Civalek (2006) developed the discrete singular convolution (DSC) algorithm for determining the frequencies of the free vibration of laminated conical shells by using a numerical solution of the governing differential equations of motion based on Loves first approximation thin shell theory. The discrete singular convolution (DSC) method was expanded by Civalek (2008) for static analysis of thick symmetric cross-ply laminated composite plates based on the first-order shear deformation theory of Whitney and Pagano. Regularized Shannons delta (RSD) kernel and Lagrange delta sequence (LDS) kernel were selected as singular convolution to illustrate the present algorithm. Gürses *et al*. (2009) investigated free vibration of laminated skew plates. Discrete singular convolution (DSC) method was used for numerical solution of vibration problems. Large deflection analysis of laminated composite plates was perused by Baltacıoglu *et al*. (2010). Nonlinear governing equation for bending based on first-order shear deformation theory (FSDT) in the von Karman sense was presented. These equations had been solved by the method of discrete singular convolution (DSC). Regularized Shannons delta (RSD) kernel and Lagrange delta sequence (LDS) kernel were selected as singular convolution to illustrate the present algorithm. Civalek *et al*. (2010) presented buckling analysis of rectangular plates subjected to various in-plane compressive loads using Kirchhoff plate theory. The method of discrete singular convolution had adopted. Linearly varying, uniform and non-uniform distributed load

*Corresponding author, Assistant Professor
E-mail: yaser_sadeghi_83@yahoo.com
[a] Associate Professor
E-mail: sohrabi@hamoon.usb.ac.ir
[b] Assistant Professor
E-mail: mojtaba.mosavi@birjand.ac.ir

Copyright © 2020 Techno-Press, Ltd.

ISSN: 1225-4568 (Print), 1598-6217 (Online)

conditions were considered on two-opposite edges for buckling. Baltacıoglu *et al*. (2011) in a paper presented nonlinear static analysis of a rectangular laminated composite thick plate resting on nonlinear two-parameter elastic foundation with cubic nonlinearity. The plate formulation was based on first-order shear deformation theory (FSDT). The nonlinear static deflections of laminated plates on elastic foundation were investigated using the discrete singular convolution method. A unified analytical method based on the first-order shear deformation theory was developed for the vibration analysis of moderately thick composite laminated cylindrical shells subjected to general boundary conditions and arbitrary intermediate ring supports, and various lamination schemes by Jin *et al*. (2013). Talebitooti (2013) in one of his paper focused on the free vibration analysis of thick, rotating laminated composite conical shells with different boundary conditions based on the three-dimensional theory, using the layerwise differential quadrature method (LW-DQM). Xiang and Chen (2014) examined meshless local collocation method for natural frequencies and mode shapes of laminated composite shells. Shen (2012) studied thermal buckling and postbuckling behavior of functionally graded carbon nanotube-reinforced composite cylindrical shells. They considered two kinds of carbon nanotube-reinforced composite (CNTRC) shells, namely, uniformly distributed (UD) and functionally graded (FG) reinforcements. The material properties of FG-CNTRCs are assumed to be graded in the thickness direction, and are estimated through a micromechanical model. The governing equations are based on a higher order shear deformation theory with a von Kármán-type of kinematic nonlinearity. Elasticity solution of functionally graded carbon nanotube-reinforced composite cylindrical panel subjected to thermomechanical load was investigated by Alibeigloo (2016). Axisymmetrical bending of single and multi-span functionally graded hollow cylinders was studied by Bian and Wang (2013). Lei *et al*. (2013) carried out buckling analysis of functionally graded carbon nanotube-reinforced composite plates using the element-free kp-Ritz method. They applied the first-order shear deformation plate theory and a set of mesh-free kernel particle functions used to approximate two-dimensional displacement fields. Effective properties of materials of the plates reinforced by single-walled carbon nanotubes (SWCNTs) are estimated through a micromechanical model based on either the Eshelby–Mori–Tanaka approach or the extended rule of mixture. Nonlinear forced vibration analysis of functionally graded carbon nanotube-reinforced composite Timoshenko beams was proposed by Ansari *et al*. (2014). Wu and Liu (2016) developed a state space meshless method for the 3D analysis of FGM axisymmetric circular plates. Free vibration analysis of rotating functionally graded carbon nanotube-reinforced composite truncated conical shells was studied by Heydarpour *et al*. (2014). Ghannad *et al*. (2012) performed Elastic analysis of pressurized thick truncated conical shells made of functionally graded materials. Zhang (2017) investigated an element-free based IMLS-Ritz method for buckling analysis of nanocomposite plates of polygonal planform. He examined the buckling behavior of nanocomposite plates of polygonal planform under in-plane loads. The plate under consideration is reinforced by single-walled carbon nanotubes (CNTs). The governing eigenvalue equation to this problem is derived based on the first-order shear deformation plate theory (FSDT) with a set of element-free shape functions in approximating the two-dimensional displacement fields. To solve this eigenvalue equation, the element-free IMLS-Ritz method is employed to furnish the buckling solution. Elastodynamic analysis of quadrilateral CNT-reinforced functionally graded composite plates using FSDT element-free method was carried out by Zhang *et al*. (2016). Liaw (2006) analysis of the surface plasmon resonance of a single core-shelled nanocomposite by surface integral equations. He investigates the interactions of an illuminating light with a single nanocomposite (a core-shelled nanoparticle) in the range of ultraviolet (UV) to near infrared (NIR), a set of new surface integral equations was derived from the Stratton–Chu formulation of Maxwells equations for a two-dimensional TM-mode problem. These integral equations belong to Fredholm equations of the second kind. Using the boundary-element method (BEM), these equations are solved to obtain the surface components (the tangential magnetic field, the normal displacement field and the tangential electric field) along the multi-connected interfaces (host/shell and shell/core) simultaneously.

In recent decade, Meshless Local Petrov-Galerkin (MLPG) method has become very useful and effective solving method in cylindrical shell for nanocomposite material because these materials have variable mechanical properties and this method doesnt require to the mesh generation on the domain. The MLPG concept was presented first by Atluri and Zhu (1998). They solved elasto-static problems in two dimensional domains. Liew *et al*. (2004) investigated the active control of laminated composite plates with piezoelectric sensor/actuator patches using an efficient mesh-free method, i.e. the element-free Galerkin (EFG) method. The formulation of the problem was based on the first-order shear deformation plate theory (FSDT) and the principle of virtual displacements. Hosseini *et al*. (2011) presented Meshless local Petrov–Galerkin method for coupled thermoelasticity analysis of a functionally graded thick hollow cylinder. In their work, coupled thermoelasticity (without energy dissipation) based on Green–Naghdi model is applied to functionally graded (FG) thick hollow cylinder. The meshless local Petrov–Galerkin method is developed to solve the boundary value problem. The Newmark finite difference method is used to treat the time dependence of the variables for transient problems. The FG cylinder is considered to be under axisymmetric and plane strain conditions and bounding surfaces of cylinder to be under thermal shock loading. Three dimensional static and dynamic analysis of thick functionally graded plates by the Meshless Local Petrov–Galerkin (MLPG) method can be found in Rezaei Mojdehi *et al*. (2011). It can be concluded from their work that the three dimensional (3D) static and dynamic analysis of thick functionally graded plates based on the Meshless Local Petrov–Galerkin (MLPG). Using the kinematics of a threedimensional continuum, the local weak form of the

equilibrium equations is derived. A weak formulation for the set of governing equations is transformed into local integral equations on local sub-domains using a Heaviside step function as test function. Also Hosseini (2012) employed Analysis of elastic wave propagation in a functionally graded thick hollow cylinder using a hybrid mesh-free method. They are presented a hybrid mesh-free method based on generalized finite difference (GFD) and Newmark finite difference (NFD) methods is presented to calculate the velocity of elastic wave propagation in functionally graded materials (FGMs). Elastic wave propagation in a functionally graded nanocomposite reinforced by carbon nanotubes employing meshless local integral equations (LIEs) was developed by Ghayoumizadeh *et al*. (2013). In their work, the transient dynamic analysis of displacement field and elastic wave propagation in finite length functionally graded nanocomposite reinforced by carbon nanotubes are carried out using local integral equations (LIEs) based on Meshless Local Petrov–Galerkin (MLPG) method. Ghadiri Rad *et al*. (2015) studied geometrically nonlinear dynamic behavior of FG thick hollow cylinder under axisymmetric mechanical shock loading using Meshless Local Petrov–Galerkin (MLPG) method. 2.5D elastic wave propagation in non-homogeneous media coupling the BEM and MLPG methods was employed by Tadeu *et al*. (2015).

The breakage of material is very difficult to simulate into some mesh based methods such as FEM is essentially based on continuum mechanics, in which the elements formulated cannot be broken. Serious error can occur because the nature of mechanical properties in nanocomposite is nonlinear, and therefore the results are highly path dependent. So, MLPG method can be successfully used for dynamic analysis of nanocomposite. In other words, MLPG method is a powerful numerical method and flexibility such as other methods like finite element method, generalized finite difference method fast accuracy of DQ or DSC method, etc.

In the present paper, the authors have extended a meshless method based on the local Petrov-Galerkin for dynamic analyses of asymmetric nanocomposite cylindrical shell. In order to discretize the derived equations in time domains, the Meshless Local Petrov-Galerkin (MLPG) method is combined with Newmark time approximation scheme. The obtained results by the MLPG method compare with analytical method, Finite Element Method (FEM) and the element free Galerkin (EFG) method. Finally, the non-symmetric nanocomposite cylindrical shell is analyzed under shock loading.

2. Governing equation

The governing equations for cylindrical shell with asymmetric geometry and boundary conditions in polar coordinates of elastic wave motion are given as follows:

$$\sigma_{r,r}+\frac{1}{r}\tau_{r\theta,\theta}+\frac{1}{r}(\sigma_r-\sigma_\theta)=\rho(r)u_{r,tt} \tag{1}$$

$$\frac{1}{r}\sigma_{\theta,\theta}+\tau_{r\theta,r}+\frac{2}{r}\tau_{r\theta}=\rho(r)u_{\theta,tt} \tag{2}$$

where $\rho(r)$ is the mass density, σ_r, σ_θ and $\tau_{r\theta}$ are radial, hoop and shear stresses, respectively. The terms u_r and u_θ denote the radial and hoop displacement, respectively.

The boundary conditions corresponding to Eqs. (1)-(2) are

Essential boundary condition: $$u_i=\bar{u}_i \quad on\ \Gamma_u \tag{3}$$

Natural boundary condition: $$\sigma_{ij}n_j=\bar{t}_i \quad on\ \Gamma_t \tag{4}$$

where $i,j=r,\theta$ and n_j is the jth component of the unit outward normal vector on the boundary. Γ_u is the essential boundary and Γ_t is the natural boundary.

In this paper, the cylindrical shell is made of a functionally graded nanocomposite reinforced by carbon nanotube (FGNRCN). The inner radius is r_{in} and outer radius is r_{out}. The carbon nanotubes (CNTs) are distributed with different angle through the thickness of the cylindrical shell of FGNRCN as some grading patterns. The effective mechanical properties of the FGNRCN cylinder can be obtained based on a micro-mechanical model as follows

$$E_1=\eta_1 V_{CNT}E_1^{CNT}+V_mE^m \tag{5}$$

$$\frac{\eta_2}{E_2}=\frac{V_{CNT}}{E_2^{CNT}}+\frac{V_m}{E^m} \tag{6}$$

$$\frac{\eta_3}{G_{12}}=\frac{V_{CNT}}{G_{12}^{CNT}}+\frac{V_m}{G^m} \tag{7}$$

$$\nu_{ij}=V_{CNT}\nu_{ij}^{CNT}+V_m\nu^m \qquad i,j=1,2,3 \qquad i\neq j \tag{8}$$

$$\rho=V_{CNT}\rho^{CNT}+V_m\rho^m \tag{9}$$

$$V_{CNT}+V_m=1 \tag{10}$$

where the terms V_{CNT} and V_m are volume fractions of carbon nanotube and matrix, respectively. The subscripts CNT and m stand for carbon nanotube and matrix, respectively. E_1^{CNT}, E_2^{CNT}, G_{12}^{CNT}, ν^{CNT}, and ρ^{CNT} are elasticity modulus, shear modulus, Poissons ratio and density of the carbon nanotubes, respectively. E^m, G^m, ν^m and ρ^m are elasticity modulus, shear modulus, Poissons ratio and density of the matrix, respectively and η_i $(i=1,2,3)$ are the CNT efficiency parameters. Four kinds of grading patterns are assumed for the carbon nanotube (CNT) volume fraction as follows:

Linear type UD: $$V_{CNT}=V_{CNT}^* \tag{11}$$

Nonlinear type V: $$V_{CNT}=2V_{CNT}^*\left(\frac{r-r_{in}}{r_{out}-r_{in}}\right) \tag{12}$$

Nonlinear type Λ: $$V_{CNT}=2V_{CNT}^*\left(\frac{r_{out}-r}{r_{out}-r_{in}}\right) \tag{13}$$

Nonlinear type X: $$V_{CNT}=4V_{CNT}^*\left|\frac{r-r_m}{r_{out}-r_{in}}\right|, \quad r_m=\frac{r_{in}+r_{out}}{2} \tag{14}$$

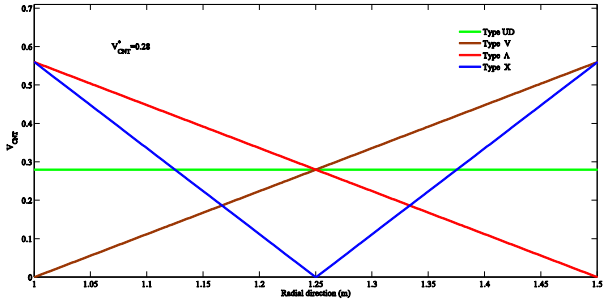

Fig. 1 Variation of nanotube volume fraction (V_{CNT}) along the radial direction for types of UD, V, Λ and X

where

$$V_{CNT}^{*}=\frac{\rho_m m_{CNT}}{m_{CNT}^2+\rho_{CNT}-\rho_{CNT}m_{CNT}} \tag{15}$$

The term m_{CNT} is the mass fraction of nanotube. Fig. 1 shows the various grading patterns can be found for $r_{in}=$ 1 m and $r_{out}=1.5$ m.

For functionally graded nanocomposite material, related stresses to strains can be written in contracted notation as

$$\begin{bmatrix}\sigma_r\\ \sigma_\theta\\ \sigma_z\\ \tau_{\theta z}\\ \tau_{zr}\\ \tau_{r\theta}\end{bmatrix}=\begin{bmatrix}C_{11}&C_{12}&C_{13}&C_{14}&C_{15}&C_{16}\\ C_{12}&C_{22}&C_{23}&C_{24}&C_{25}&C_{26}\\ C_{13}&C_{23}&C_{33}&C_{34}&C_{35}&C_{36}\\ C_{14}&C_{24}&C_{34}&C_{44}&C_{45}&C_{46}\\ C_{15}&C_{25}&C_{35}&C_{45}&C_{55}&C_{56}\\ C_{16}&C_{26}&C_{36}&C_{46}&C_{56}&C_{66}\end{bmatrix}\begin{bmatrix}\varepsilon_r\\ \varepsilon_\theta\\ \varepsilon_z\\ \gamma_{\theta z}\\ \gamma_{zr}\\ \gamma_{r\theta}\end{bmatrix} \tag{16}$$

Functionally graded nanocomposite material is an orthotropic material so the stiffness matrix, C_{ij}, for an orthotropic material in terms of the engineering constants are

$$C_{11}=\frac{1-\nu_{\theta z}\nu_{z\theta}}{E_\theta E_z\Delta}$$

$$C_{22}=\frac{1-\nu_{rz}\nu_{zr}}{E_r E_z\Delta}$$

$$C_{12}=\frac{\nu_{\theta r}+\nu_{zr}\nu_{\theta z}}{E_\theta E_z\Delta}=\frac{\nu_{r\theta}+\nu_{z\theta}\nu_{rz}}{E_r E_z\Delta}$$

$$C_{23}=\frac{\nu_{z\theta}+\nu_{r\theta}\nu_{zr}}{E_r E_z\Delta}=\frac{\nu_{\theta z}+\nu_{\theta r}\nu_{rz}}{E_r E_\theta\Delta} \tag{17}$$

$$C_{13}=\frac{\nu_{zr}+\nu_{\theta r}\nu_{z\theta}}{E_\theta E_z\Delta}=\frac{\nu_{rz}+\nu_{r\theta}\nu_{\theta z}}{E_r E_\theta\Delta}$$

$$C_{33}=\frac{1-\nu_{r\theta}\nu_{\theta r}}{E_r E_\theta\Delta}$$

$$C_{44}=G_{\theta z}\qquad C_{55}=G_{zr}$$

$$C_{66}=G_{r\theta}$$

where

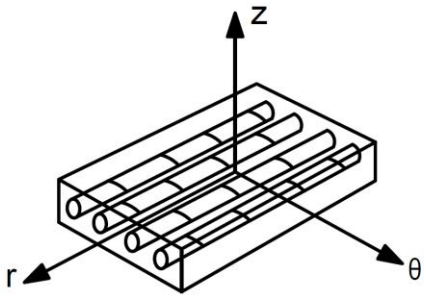

Fig. 2 The unidirectional reinforced lamina

$$\Delta=\frac{1-\nu_{r\theta}\nu_{\theta r}-\nu_{\theta z}\nu_{z\theta}-\nu_{zr}\nu_{rz}-2\nu_{\theta r}\nu_{z\theta}\nu_{rz}}{E_r E_\theta E_z} \tag{18}$$

$$\frac{\nu_{ij}}{E_i}=\frac{\nu_{ji}}{E_j}\qquad i,j=r,\theta,z \tag{19}$$

For a unidirectional reinforced lamina in the $r-\theta$ plane shown in Fig. 2, a plane strain state is defined by setting

$$\varepsilon_z=0?\qquad \gamma_{\theta z}=\qquad \gamma_{zr}= \tag{20}$$

so that

$$\varepsilon_r\neq 0?\qquad \varepsilon_\theta\neq\qquad \gamma_{r\theta}\neq \tag{21}$$

The stresses and strains were defined in the principal material coordinates for an orthotropic material. However, the principal directions of orthotropic materials often do not coincide with coordinate directions that they are geometrically natural to the solution of the problem. For example Fig. 3 can be seen. Thus, a relation is needed between the stresses and strains in the principal material coordinates and those are in the body coordinates. At this point, we recall from elementary mechanics of materials in the transformation equations for expressing stresses in a $r-\theta$ coordinate system. The transformation matrix is shown as follow.

$$[T]=\begin{bmatrix}cos^2\alpha & sin^2\alpha & 2sin\alpha\ cos\alpha\\ sin^2\alpha & cos^2\alpha & -2sin\alpha\ cos\alpha\\ -sin\alpha\ cos\alpha & sin\alpha\ cos\alpha & cos^2\alpha-sin^2\alpha\end{bmatrix} \tag{22}$$

however, if the simple matrix

$$[\varrho]=\begin{bmatrix}1&0&0\\0&1&0\\0&0&2\end{bmatrix} \tag{23}$$

then the engineering strain vectors can be used instead of the tensor strain vectors in the strain transformation as well as in stress-strain low transformation.

$$\begin{bmatrix}\varepsilon_r\\ \varepsilon_\theta\\ \gamma_{r\theta}\end{bmatrix}=[\varrho]\begin{bmatrix}\varepsilon_r\\ \varepsilon_\theta\\ \frac{\gamma_{r\theta}}{2}\end{bmatrix} \tag{24}$$

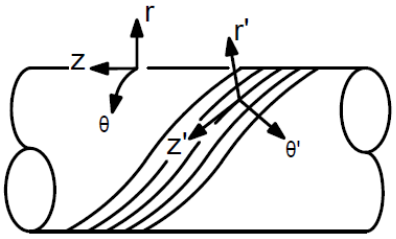

Fig. 3 Helically wound fiber reinforced circular cylindrical shell

However, $[\varrho][T][\varrho]^{-1}$ can be shown to be $[T]^{-T}$ where the superscript T denotes the matrix transpose. Then, if we use the abbreviation

$$[\varrho][T][\varrho]^{-1} = [T]^{-T} \tag{25}$$

$$[\bar{Q}] = [T]^{-1}[Q][T]^{-T} \tag{26}$$

The stress-strain relations in $r-\theta$ coordinates for functionally graded nanocomposite material with different angle are

$$\begin{bmatrix} \sigma_r \\ \sigma_\theta \\ \tau_{r\theta} \end{bmatrix} = \left[\bar{Q}\right] \begin{bmatrix} \varepsilon_r \\ \varepsilon_\theta \\ \gamma_{r\theta} \end{bmatrix} = \begin{bmatrix} \bar{Q}_{11} & \bar{Q}_{12} & \bar{Q}_{16} \\ \bar{Q}_{12} & \bar{Q}_{22} & \bar{Q}_{26} \\ \bar{Q}_{16} & \bar{Q}_{26} & \bar{Q}_{66} \end{bmatrix} \begin{bmatrix} \varepsilon_r \\ \varepsilon_\theta \\ \gamma_{r\theta} \end{bmatrix} \tag{27}$$

in which

$$\begin{aligned}
\bar{Q}_{11} &= Q_{11}cos^4\alpha \\
&+2\left(Q_{12}+2Q_{66}\right)sin^2\alpha cos^2\alpha + Q_{22}sin^4\alpha \\
\bar{Q}_{12} &= \left(Q_{11}+Q_{22}-4Q_{66}\right)sin^2\alpha cos^2\alpha \\
&+Q_{12}\left(sin^4\alpha+cos^4\alpha\right) \\
\bar{Q}_{22} &= Q_{11}sin^4\alpha \\
&+2\left(Q_{12}+2Q_{66}\right)sin^2\alpha cos^2\alpha + Q_{22}cos^4\alpha \\
\bar{Q}_{16} &= \left(Q_{11}-Q_{12}-2Q_{66}\right)sin\alpha cos^3\alpha \\
&+\left(Q_{12}-Q_{22}+2Q_{66}\right)sin^3\alpha cos\alpha \\
\bar{Q}_{26} &= \left(Q_{11}-Q_{12}-2Q_{66}\right)sin^3\alpha cos\alpha \\
&+\left(Q_{12}-Q_{22}+2Q_{66}\right)sin\alpha cos^3\alpha \\
\bar{Q}_{66} &= \left(Q_{11}+Q_{22}-2Q_{12}-2Q_{66}\right)sin^2\alpha cos^2\alpha \\
&+Q_{66}\left(sin^4\alpha+cos^4\alpha\right)
\end{aligned} \tag{28}$$

in Eq. (28) Q_{11}, Q_{22}, Q_{12} and Q_{66} define as follows

$$Q_{11} = \frac{E_r\left(1-\nu_{r\theta}\right)\left(1-\nu_{\theta r}\right)}{\left(1-\nu_{r\theta}-\nu_{\theta r}\right)\left(1-\nu_{r\theta}\nu_{\theta r}\right)} \tag{29}$$

$$Q_{22} = \frac{E_\theta\left(1-\nu_{r\theta}\right)\left(1-\nu_{\theta r}\right)}{\left(1-\nu_{r\theta}-\nu_{\theta r}\right)\left(1-\nu_{r\theta}\nu_{\theta r}\right)}$$

$$Q_{12} = \frac{E_r\left(1-\nu_{r\theta}\right)\nu_{\theta r}}{\left(1-\nu_{r\theta}-\nu_{\theta r}\right)\left(1-\nu_{r\theta}\nu_{\theta r}\right)}$$

$$= \frac{E_\theta\left(1-\nu_{\theta r}\right)\nu_{r\theta}}{\left(1-\nu_{r\theta}-\nu_{\theta r}\right)\left(1-\nu_{r\theta}\nu_{\theta r}\right)}$$

$$Q_{66} = G_{r\theta}$$

The strain–displacement relations are given by

$$\varepsilon_r = u_{r,r} \tag{30}$$

$$\varepsilon_\theta = \frac{1}{r}\left(u_{\theta,\theta}+u_r\right) \tag{31}$$

$$\gamma_{r\theta} = \frac{1}{r}u_{r,\theta}+u_{\theta,r}-\frac{1}{r}u_\theta \tag{32}$$

where ε_r, ε_θ and $\gamma_{r\theta}$ are radial, hoop and shear strain, respectively.

3. Meshfree local integral equations

Based on the local weighted residual method, the weak-form for Eqs. (1)-(2) over a local subdomains Ω_Q (integration) instead of constructing the global weak-form for whole domain of dynamic problem can be stated as

$$\int_{\Omega_Q} rW_I\left(\sigma_{r,r}+\frac{\left(\sigma_r-\sigma_\theta\right)}{r}+\frac{1}{r}\tau_{r\theta,\theta}-\rho(r)u_{r,tt}\right)d\Omega = 0 \tag{33}$$

$$\int_{\Omega_Q} rW_I\left(\frac{1}{r}\sigma_{\theta,\theta}+\tau_{r\theta,r}+\frac{2\tau_{r\theta}}{r}-\rho(r)u_{\theta,tt}\right)d\Omega = 0 \tag{34}$$

where W_I is the weight function and we use the same weight function for all the equations involved. Using the divergence theory for Eqs. (33)-(34) as follows

$$\begin{aligned}
&\int_{\Omega_Q}\left(rW_{I,r}\sigma_r+W_I\sigma_\theta+W_{I,\theta}\tau_{r\theta}\right)d\Omega-\int_{\Gamma_Q} rW_I\left(n_r\sigma_r+\frac{n_\theta}{r}\tau_{r\theta}\right)d\Gamma \\
&+\int_{\Omega_Q} rW_I\rho(r)u_{r,tt}d\Omega = 0
\end{aligned} \tag{35}$$

$$\begin{aligned}
&\int_{\Omega_Q}\left(W_{I,\theta}\sigma_\theta+rW_{I,r}\tau_{r\theta}-W_I\tau_{r\theta}\right)d\Omega-\int_{\Gamma_Q} rW_I\left(\frac{n_\theta}{r}\sigma_\theta+n_r\tau_{r\theta}\right)d\Gamma \\
&+\int_{\Omega_Q} rW_I\rho(r)u_{\theta,tt}d\Omega = 0
\end{aligned} \tag{36}$$

where Ω_Q and Γ_Q are quadrature domain and boundary of quadrature domain, respectively. n_r and n_θ

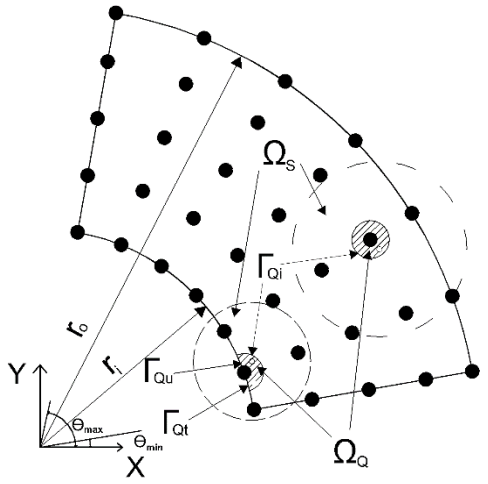

Fig. 4 The domain and the boundary of cylindrical structure in MLPG method

are the unit outward normal vectors on the boundary for r and θ direction, respectively. The boundary of quadrature domain is divided to some parts as $\Gamma_Q = \Gamma_{Q_i} \cup \Gamma_{Q_u} \cup \Gamma_{Q_t}$. The term Γ_{Q_i} is the internal boundary of the quadrature domain, Γ_{Q_u} is the part of the essential boundary that intersects with the quadrature domain and Γ_{Q_t} is the part of the natural boundary that intersects with the quadrature domain (see Fig. 4).

Then we can change the expression of Eqs. (35)-(36) to

$$\begin{aligned}
&\int_{\Omega_Q} \left(rW_{I,r}\sigma_r + W_I\sigma_\theta + W_{I,\theta}\tau_{r\theta} \right) d\Omega \\
&- \int_{\Gamma_{Q_i}} rW_I \left(n_r\sigma_r + \frac{n_\theta}{r}\tau_{r\theta} \right) d\Gamma \\
&\quad - \int_{\Gamma_{Q_u}} rW_I \left(n_r\sigma_r + \frac{n_\theta}{r}\tau_{r\theta} \right) d\Gamma \\
&\quad + \int_{\Omega_Q} rW_I\rho(r)u_{r,tt}d\Omega = \int_{\Gamma_{Q_t}} rW_I t_r d\Gamma
\end{aligned} \tag{37}$$

$$\begin{aligned}
&\int_{\Omega_Q} \left(W_{I,\theta}\sigma_\theta + rW_{I,r}\tau_{r\theta} - W_I\tau_{r\theta} \right) d\Omega \\
&- \int_{\Gamma_{Q_i}} rW_I \left(\frac{n_\theta}{r}\sigma_\theta + n_r\tau_{r\theta} \right) d\Gamma \\
&\quad - \int_{\Gamma_{Q_u}} rW_I \left(\frac{n_\theta}{r}\sigma_\theta + n_r\tau_{r\theta} \right) d\Gamma \\
&\quad + \int_{\Omega_Q} rW_I\rho(r)u_{\theta,tt}d\Omega = \int_{\Gamma_{Q_t}} rW_I t_\theta d\Gamma
\end{aligned} \tag{38}$$

where t_r and t_θ are the radial and hoop tractions, respectively and they are defined as follows:

Table 1 Typical conventional from of radial basis function

Item	Name	Expression	Shape Parameters
1	Multi quadrics (MQ)	$R_i(\bar{r}) = (\bar{r}^2 + C^2)^q$	C, q
2	Gaussian (EXP)	$R_i(\bar{r}) = exp(-c\bar{r}^2)$	c
3	Thin plate spline (TPS)	$R_i(\bar{r}) = \bar{r}^\varsigma$	ς
4	Logarithmic RBF	$R_i(\bar{r}) = \bar{r}^\varsigma \log\bar{r}$	ς

$$t_r = n_r\sigma_r + \frac{n_\theta}{r}\tau_{r\theta} \tag{39}$$

$$t_\theta = n_r\tau_{r\theta} + \frac{n_\theta}{r}\sigma_\theta \tag{40}$$

The displacements can be approximated using the shape function. The shape function is defined for each point using the nodes in support domain Ω_s of a point (see Fig. 4). The creation of MLPG shape functions is the central and most important issue in the MLPG methods. With development of more effective methods for constructing shape functions but yet one of the best methods is Radial Point Interpolation Method (RPIM) shape function. In this paper, we used RPIM shape function, the advantages of using this shape function are, the nodal distribution can be arbitrary within reason, the algorithm is stable, it possesses the Kronecker delta function property and the field approximation using the shape function is compatible throughout the problem domain. We choose radial functions as the basis in equation

$$u^h\left(\bar{r}, \bar{r}_Q\right) = \sum_{i=1}^{n} R_i\left(\bar{r}\right)\Theta_i\left(\bar{r}_Q\right) = \boldsymbol{R}^T\left(\bar{r}\right)\boldsymbol{\Theta}\left(\bar{r}_Q\right) \tag{41}$$

where vector $\boldsymbol{\Theta}$ is defined in Eq. (42), and R_i is a radial basis function with $\bar{r}$ the distance between point x and x_I, so we have

$$\boldsymbol{\Theta}^T\left(\bar{r}_Q\right) = \left\{\Theta_1, \Theta_2, \Theta_3, \ldots, \Theta_n\right\} \tag{42}$$

$$\bar{r} = \left[r^2 + r_I^2 - 2r r_I \cos\left(\theta - \theta_I\right) \right]^{1/2} \tag{43}$$

The vector $\boldsymbol{R}$ has the form:

$$\boldsymbol{R}^T\left(\bar{r}\right) = \left\{R_1\left(\bar{r}\right), R_2\left(\bar{r}\right), R_3\left(\bar{r}\right), \ldots, R_n\left(\bar{r}\right)\right\} \tag{44}$$

There are a number of forms of Radial Basis Functions (RBF) used by the mathematics community. Table 1 lists the four most often used forms of radial functions with some shape parameters that can be tuned for better performance.

In this paper we used the type of a classical form is called multiquadric (MQ) basis. The MQ basis function is following

$$R_i\left(\bar{r}\right)=\left(\bar{r}^2+C^2\right)^q \tag{45}$$

where C and q are constant coefficient. The matrix $\boldsymbol{R}_Q$ can be written:

$$\boldsymbol{R}_Q=\begin{bmatrix} R_1\left(\bar{r}_1\right) & R_2\left(\bar{r}_1\right) & \dots & R_n\left(\bar{r}_1\right) \\ R_1\left(\bar{r}_2\right) & R_2\left(\bar{r}_2\right) & \dots & R_n\left(\bar{r}_2\right) \\ \vdots & \vdots & \ddots & \vdots \\ R_1\left(\bar{r}_n\right) & R_2\left(\bar{r}_n\right) & \dots & R_n\left(\bar{r}_n\right) \end{bmatrix} \tag{46}$$

where

$$\bar{r}_k=\left[r_k^2+r_I^2-2r_k ?r_I \qquad \left(\theta_k-\theta_I\right)\right]^{1/2} \tag{47}$$

Because the distance is directionless, we should have

$$R_i\left(\bar{r}_j\right)=R_j\left(\bar{r}_i\right) \tag{48}$$

Therefore, the moment matrix $\boldsymbol{R}_Q$ is symmetric.

The vectors of coefficients $\boldsymbol{\Theta}$ in Eq. (41) are determined by enforcing that the interpolation passes through all the n nodes within the support domain. The interpolation at the kth point has the form:

$$u_k=u\left(r_k,\theta_k\right)=\sum_{i=1}^{n}\Theta_i R_i\left(r_k,\theta_k\right)?\ k= \qquad \dots\ n \tag{49}$$

or in matrix form:

$$\boldsymbol{U}_s=\boldsymbol{R}_Q\boldsymbol{\Theta} \tag{50}$$

where $\boldsymbol{U}_s$ is the vector that collects all the field nodal variables at the n nodes in the support domain. A unique solution for vectors of coefficients $\boldsymbol{\Theta}$ is obtained if the inverse of $\boldsymbol{R}_Q$ exists:

$$\boldsymbol{\Theta}=\boldsymbol{R}_Q^{-1}\boldsymbol{U}_s \tag{51}$$

Furthermore, shape function $\varphi(\bar{r})$ is defined as follow:

$$\varphi\left(\bar{r}\right)=\boldsymbol{R}^T\left(\bar{r}\right)\boldsymbol{R}_Q^{-1} \tag{52}$$

so the Eq. (41) can be written

$$u^h\left(\bar{r},\bar{r}_Q\right)=\varphi?\left(\bar{r}\right)\bar{u} \tag{53}$$

Substitution of the Eq. (27) into Eqs. (37)-(38) gives

$$\begin{gathered}\int_{\Omega_Q}\left[rW_{I,r}(\bar{Q}_{11}\varepsilon_r+\bar{Q}_{12}\varepsilon_\theta+\bar{Q}_{16}\gamma_{r\theta})+W_I(\bar{Q}_{12}\varepsilon_r+\right.\\ \bar{Q}_{22}\varepsilon_\theta+\bar{Q}_{26}\gamma_{r\theta})+W_{I,\theta}(\bar{Q}_{16}\varepsilon_r+\bar{Q}_{26}\varepsilon_\theta+\\ \left.\bar{Q}_{66}\gamma_{r\theta})\right]d\Omega-\int_{\Gamma_{Q_i}}rW_I\left[n_r(\bar{Q}_{11}\varepsilon_r+\bar{Q}_{12}\varepsilon_\theta+\right.\\ \bar{Q}_{16}\gamma_{r\theta})+\frac{n_\theta}{r}(\bar{Q}_{16}\varepsilon_r+\bar{Q}_{26}\varepsilon_\theta+\bar{Q}_{66}\gamma_{r\theta})\Big]d\Gamma-\\ \int_{\Gamma_{Q_u}}rW_I\left[n_r(\bar{Q}_{11}\varepsilon_r+\bar{Q}_{12}\varepsilon_\theta+\bar{Q}_{16}\gamma_{r\theta})+\frac{n_\theta}{r}(\bar{Q}_{16}\varepsilon_r+\right.\\ \left.\bar{Q}_{26}\varepsilon_\theta+\bar{Q}_{66}\gamma_{r\theta})\right]d\Gamma+\int_{\Omega_Q}rW_I\rho(r)u_{r,tt}\,d\Omega=\\ \int_{\Gamma_{Q_t}}rW_I t_r\,d\Gamma\end{gathered} \tag{54}$$

$$\begin{gathered}\int_{\Omega_Q}\left[W_{I,\theta}(\bar{Q}_{12}\varepsilon_r+\bar{Q}_{22}\varepsilon_\theta+\bar{Q}_{26}\gamma_{r\theta})+rW_{I,r}(\bar{Q}_{16}\varepsilon_r+\right.\\ \bar{Q}_{26}\varepsilon_\theta+\bar{Q}_{66}\gamma_{r\theta})-W_I(\bar{Q}_{16}\varepsilon_r+\bar{Q}_{26}\varepsilon_\theta+\\ \left.\bar{Q}_{66}\gamma_{r\theta})\right]d\Omega-\int_{\Gamma_{Q_i}}rW_I\left[\frac{n_\theta}{r}(\bar{Q}_{12}\varepsilon_r+\bar{Q}_{22}\varepsilon_\theta+\right.\\ \bar{Q}_{26}\gamma_{r\theta})+n_r(\bar{Q}_{16}\varepsilon_r+\bar{Q}_{26}\varepsilon_\theta+\bar{Q}_{66}\gamma_{r\theta})\Big]d\Gamma-\\ \int_{\Gamma_{Q_u}}rW_I\left[\frac{n_\theta}{r}(\bar{Q}_{12}\varepsilon_r+\bar{Q}_{22}\varepsilon_\theta+\bar{Q}_{26}\gamma_{r\theta})+n_r(\bar{Q}_{16}\varepsilon_r+\right.\\ \left.\bar{Q}_{26}\varepsilon_\theta+\bar{Q}_{66}\gamma_{r\theta})\right]d\Gamma+\int_{\Omega_Q}rW_I\rho(r)u_{\theta,tt}\,d\Omega=\\ \int_{\Gamma_{Q_t}}rW_I t_\theta\,d\Gamma\end{gathered} \tag{55}$$

using Eqs. (30)-(32) and (53) and substitution into the Eqs. (54)-(55), we receive

$$\begin{gathered}\int_{\Omega_Q}\left\{rW_{I,r}\left[\bar{Q}_{11}\left(\left(\sum_{j=1}^{k}\frac{\partial\varphi_j}{\partial r}\right)\bar{u}_r\right)+\right.\right.\\ \bar{Q}_{12}\left(\frac{1}{r}\left(\left(\sum_{j=1}^{k}\frac{\partial\varphi_j}{\partial\theta}\right)\bar{u}_\theta+\left(\sum_{j=1}^{k}\varphi_j\right)\bar{u}_r\right)\right)+\\ \bar{Q}_{16}\left(\frac{1}{r}\left(\sum_{j=1}^{k}\frac{\partial\varphi_j}{\partial\theta}\right)\bar{u}_r+\left(\sum_{j=1}^{k}\frac{\partial\varphi_j}{\partial r}\right)\bar{u}_\theta-\right.\\ \left.\left.\frac{1}{r}\left(\sum_{j=1}^{k}\varphi_j\right)\bar{u}_\theta\right)\right]+W_I\left[\bar{Q}_{12}\left(\left(\sum_{j=1}^{k}\frac{\partial\varphi_j}{\partial r}\right)\bar{u}_r\right)+\right.\\ \bar{Q}_{22}\left(\frac{1}{r}\left(\left(\sum_{j=1}^{k}\frac{\partial\varphi_j}{\partial\theta}\right)\bar{u}_\theta+\left(\sum_{j=1}^{k}\varphi_j\right)\bar{u}_r\right)\right)+\\ \bar{Q}_{26}\left(\frac{1}{r}\left(\sum_{j=1}^{k}\frac{\partial\varphi_j}{\partial\theta}\right)\bar{u}_r+\left(\sum_{j=1}^{k}\frac{\partial\varphi_j}{\partial r}\right)\bar{u}_\theta-\right.\\ \left.\left.\frac{1}{r}\left(\sum_{j=1}^{k}\varphi_j\right)\bar{u}_\theta\right)\right]+W_{I,\theta}\left[\bar{Q}_{16}\left(\left(\sum_{j=1}^{k}\frac{\partial\varphi_j}{\partial r}\right)\bar{u}_r\right)+\right.\\ \bar{Q}_{26}\left(\frac{1}{r}\left(\left(\sum_{j=1}^{k}\frac{\partial\varphi_j}{\partial\theta}\right)\bar{u}_\theta+\left(\sum_{j=1}^{k}\varphi_j\right)\bar{u}_r\right)\right)+\\ \bar{Q}_{66}\left(\frac{1}{r}\left(\sum_{j=1}^{k}\frac{\partial\varphi_j}{\partial\theta}\right)\bar{u}_r+\left(\sum_{j=1}^{k}\frac{\partial\varphi_j}{\partial r}\right)\bar{u}_\theta-\right.\\ \left.\left.\left.\frac{1}{r}\left(\sum_{j=1}^{k}\varphi_j\right)\bar{u}_\theta\right)\right]\right\}d\Omega-\\ \int_{\Gamma_{Q_i}}rW_I\left\{n_r\left[\bar{Q}_{11}\left(\left(\sum_{j=1}^{k}\frac{\partial\varphi_j}{\partial r}\right)\bar{u}_r\right)+\right.\right.\\ \bar{Q}_{12}\left(\frac{1}{r}\left(\left(\sum_{j=1}^{k}\frac{\partial\varphi_j}{\partial\theta}\right)\bar{u}_\theta+\left(\sum_{j=1}^{k}\varphi_j\right)\bar{u}_r\right)\right)+\\ \bar{Q}_{16}\left(\frac{1}{r}\left(\sum_{j=1}^{k}\frac{\partial\varphi_j}{\partial\theta}\right)\bar{u}_r+\left(\sum_{j=1}^{k}\frac{\partial\varphi_j}{\partial r}\right)\bar{u}_\theta-\right.\\ \left.\left.\frac{1}{r}\left(\sum_{j=1}^{k}\varphi_j\right)\bar{u}_\theta\right)\right]+\frac{n_\theta}{r}\left[\bar{Q}_{16}\left(\left(\sum_{j=1}^{k}\frac{\partial\varphi_j}{\partial r}\right)\bar{u}_r\right)+\right.\\ \bar{Q}_{26}\left(\frac{1}{r}\left(\left(\sum_{j=1}^{k}\frac{\partial\varphi_j}{\partial\theta}\right)\bar{u}_\theta+\left(\sum_{j=1}^{k}\varphi_j\right)\bar{u}_r\right)\right)+\\ \bar{Q}_{66}\left(\frac{1}{r}\left(\sum_{j=1}^{k}\frac{\partial\varphi_j}{\partial\theta}\right)\bar{u}_r+\left(\sum_{j=1}^{k}\frac{\partial\varphi_j}{\partial r}\right)\bar{u}_\theta-\right.\\ \left.\left.\left.\frac{1}{r}\left(\sum_{j=1}^{k}\varphi_j\right)\bar{u}_\theta\right)\right]\right\}d\Gamma-\\ \int_{\Gamma_{Q_u}}rW_I\left\{n_r\left[\bar{Q}_{11}\left(\left(\sum_{j=1}^{k}\frac{\partial\varphi_j}{\partial r}\right)\bar{u}_r\right)+\right.\right.\\ \bar{Q}_{12}\left(\frac{1}{r}\left(\left(\sum_{j=1}^{k}\frac{\partial\varphi_j}{\partial\theta}\right)\bar{u}_\theta+\left(\sum_{j=1}^{k}\varphi_j\right)\bar{u}_r\right)\right)+\\ \bar{Q}_{16}\left(\frac{1}{r}\left(\sum_{j=1}^{k}\frac{\partial\varphi_j}{\partial\theta}\right)\bar{u}_r+\left(\sum_{j=1}^{k}\frac{\partial\varphi_j}{\partial r}\right)\bar{u}_\theta-\right.\end{gathered} \tag{56}$$

$$\frac{1}{r}\left(\sum_{j=1}^{k}\varphi_j\right)\bar{u}_\theta\Big)\Big] + \frac{n_\theta}{r}\Big[\bar{Q}_{16}\Big(\Big(\sum_{j=1}^{k}\frac{\partial\varphi_j}{\partial r}\Big)\bar{u}_r\Big) + \bar{Q}_{26}\Big(\frac{1}{r}\Big(\Big(\sum_{j=1}^{k}\frac{\partial\varphi_j}{\partial\theta}\Big)\bar{u}_\theta + \Big(\sum_{j=1}^{k}\varphi_j\Big)\bar{u}_r\Big)\Big) + \bar{Q}_{66}\Big(\frac{1}{r}\Big(\sum_{j=1}^{k}\frac{\partial\varphi_j}{\partial\theta}\Big)\bar{u}_r + \Big(\sum_{j=1}^{k}\frac{\partial\varphi_j}{\partial r}\Big)\bar{u}_\theta - \frac{1}{r}\Big(\sum_{j=1}^{k}\varphi_j\Big)\bar{u}_\theta\Big)\Big]\Big\}d\Gamma + \int_{\Omega_Q} rW_I\rho(r)u_{r,tt}\,d\Omega = \int_{\Gamma_{Q_t}} rW_I t_r\,d\Gamma$$

$$\begin{aligned}
&\int_{\Omega_Q}\Big\{W_{I,\theta}\Big[\bar{Q}_{12}\Big(\Big(\sum_{j=1}^{k}\frac{\partial\varphi_j}{\partial r}\Big)\bar{u}_r\Big) + \bar{Q}_{22}\Big(\frac{1}{r}\Big(\Big(\sum_{j=1}^{k}\frac{\partial\varphi_j}{\partial\theta}\Big)\bar{u}_\theta + \Big(\sum_{j=1}^{k}\varphi_j\Big)\bar{u}_r\Big)\Big) + \bar{Q}_{26}\Big(\frac{1}{r}\Big(\sum_{j=1}^{k}\frac{\partial\varphi_j}{\partial\theta}\Big)\bar{u}_r + \Big(\sum_{j=1}^{k}\frac{\partial\varphi_j}{\partial r}\Big)\bar{u}_\theta - \frac{1}{r}\Big(\sum_{j=1}^{k}\varphi_j\Big)\bar{u}_\theta\Big)\Big] + rW_{I,r}\Big[\bar{Q}_{16}\Big(\Big(\sum_{j=1}^{k}\frac{\partial\varphi_j}{\partial r}\Big)\bar{u}_r\Big) + \bar{Q}_{26}\Big(\frac{1}{r}\Big(\Big(\sum_{j=1}^{k}\frac{\partial\varphi_j}{\partial\theta}\Big)\bar{u}_\theta + \Big(\sum_{j=1}^{k}\varphi_j\Big)\bar{u}_r\Big)\Big) + \bar{Q}_{66}\Big(\frac{1}{r}\Big(\sum_{j=1}^{k}\frac{\partial\varphi_j}{\partial\theta}\Big)\bar{u}_r + \Big(\sum_{j=1}^{k}\frac{\partial\varphi_j}{\partial r}\Big)\bar{u}_\theta - \frac{1}{r}\Big(\sum_{j=1}^{k}\varphi_j\Big)\bar{u}_\theta\Big)\Big] - W_I\Big[\bar{Q}_{16}\Big(\Big(\sum_{j=1}^{k}\frac{\partial\varphi_j}{\partial r}\Big)\bar{u}_r\Big) + \bar{Q}_{26}\Big(\frac{1}{r}\Big(\Big(\sum_{j=1}^{k}\frac{\partial\varphi_j}{\partial\theta}\Big)\bar{u}_\theta + \Big(\sum_{j=1}^{k}\varphi_j\Big)\bar{u}_r\Big)\Big) + \bar{Q}_{66}\Big(\frac{1}{r}\Big(\sum_{j=1}^{k}\frac{\partial\varphi_j}{\partial\theta}\Big)\bar{u}_r + \Big(\sum_{j=1}^{k}\frac{\partial\varphi_j}{\partial r}\Big)\bar{u}_\theta - \frac{1}{r}\Big(\sum_{j=1}^{k}\varphi_j\Big)\bar{u}_\theta\Big)\Big]\Big\}d\Omega - \\
&\int_{\Gamma_{Q_i}} rW_I\Big\{\frac{n_\theta}{r}\Big[\bar{Q}_{12}\Big(\Big(\sum_{j=1}^{k}\frac{\partial\varphi_j}{\partial r}\Big)\bar{u}_r\Big) + \bar{Q}_{22}\Big(\frac{1}{r}\Big(\Big(\sum_{j=1}^{k}\frac{\partial\varphi_j}{\partial\theta}\Big)\bar{u}_\theta + \Big(\sum_{j=1}^{k}\varphi_j\Big)\bar{u}_r\Big)\Big) + \bar{Q}_{26}\Big(\frac{1}{r}\Big(\sum_{j=1}^{k}\frac{\partial\varphi_j}{\partial\theta}\Big)\bar{u}_r + \Big(\sum_{j=1}^{k}\frac{\partial\varphi_j}{\partial r}\Big)\bar{u}_\theta - \frac{1}{r}\Big(\sum_{j=1}^{k}\varphi_j\Big)\bar{u}_\theta\Big)\Big] + n_r\Big[\bar{Q}_{16}\Big(\Big(\sum_{j=1}^{k}\frac{\partial\varphi_j}{\partial r}\Big)\bar{u}_r\Big) + \bar{Q}_{26}\Big(\frac{1}{r}\Big(\Big(\sum_{j=1}^{k}\frac{\partial\varphi_j}{\partial\theta}\Big)\bar{u}_\theta + \Big(\sum_{j=1}^{k}\varphi_j\Big)\bar{u}_r\Big)\Big) + \bar{Q}_{66}\Big(\frac{1}{r}\Big(\sum_{j=1}^{k}\frac{\partial\varphi_j}{\partial\theta}\Big)\bar{u}_r + \Big(\sum_{j=1}^{k}\frac{\partial\varphi_j}{\partial r}\Big)\bar{u}_\theta - \frac{1}{r}\Big(\sum_{j=1}^{k}\varphi_j\Big)\bar{u}_\theta\Big)\Big]\Big\}d\Gamma - \\
&\int_{\Gamma_{Q_u}} rW_I\Big\{\frac{n_\theta}{r}\Big[\bar{Q}_{12}\Big(\Big(\sum_{j=1}^{k}\frac{\partial\varphi_j}{\partial r}\Big)\bar{u}_r\Big) + \bar{Q}_{22}\Big(\frac{1}{r}\Big(\Big(\sum_{j=1}^{k}\frac{\partial\varphi_j}{\partial\theta}\Big)\bar{u}_\theta + \Big(\sum_{j=1}^{k}\varphi_j\Big)\bar{u}_r\Big)\Big) + \bar{Q}_{26}\Big(\frac{1}{r}\Big(\sum_{j=1}^{k}\frac{\partial\varphi_j}{\partial\theta}\Big)\bar{u}_r + \Big(\sum_{j=1}^{k}\frac{\partial\varphi_j}{\partial r}\Big)\bar{u}_\theta - \frac{1}{r}\Big(\sum_{j=1}^{k}\varphi_j\Big)\bar{u}_\theta\Big)\Big] + n_r\Big[\bar{Q}_{16}\Big(\Big(\sum_{j=1}^{k}\frac{\partial\varphi_j}{\partial r}\Big)\bar{u}_r\Big) + \bar{Q}_{26}\Big(\frac{1}{r}\Big(\Big(\sum_{j=1}^{k}\frac{\partial\varphi_j}{\partial\theta}\Big)\bar{u}_\theta + \Big(\sum_{j=1}^{k}\varphi_j\Big)\bar{u}_r\Big)\Big) + \bar{Q}_{66}\Big(\frac{1}{r}\Big(\sum_{j=1}^{k}\frac{\partial\varphi_j}{\partial\theta}\Big)\bar{u}_r + \Big(\sum_{j=1}^{k}\frac{\partial\varphi_j}{\partial r}\Big)\bar{u}_\theta - \frac{1}{r}\Big(\sum_{j=1}^{k}\varphi_j\Big)\bar{u}_\theta\Big)\Big]\Big\}d\Gamma + \int_{\Omega_Q} rW_I\rho(r)u_{\theta,tt}\,d\Omega = \int_{\Gamma_{Q_t}} rW_I t_\theta\,d\Gamma
\end{aligned} \tag{57}$$

4. Time domain analysis

In order to discretize Eqs. (56)-(57) in time domains, in this article, the Newmark time approximation scheme with suitable time step is used. Consider the governing equation of non-dimensional time $\bar{t} = t_p$ of system takes the form

$$[M]\{\ddot{u}^{t_p}\} + [K]\{u^{t_p}\} = \{F^{t_p}\} \tag{58}$$

F^0 and u^0, are the initial conditions so the following equation can be obtained

$$[M]\{\ddot{u}^0\} = \{F^0\} - [K]\{u^0\} \tag{59}$$

The matrix $[K_m]$ and the vector $\left\{F_m^{t_p}\right\}$ are defined as follows

$$[K_m] = [K] + \frac{1}{\lambda_1\Delta t^2}[M] \tag{60}$$

$$\left\{F_m^{t_p}\right\} = \{F^{t_p}\} + \frac{1}{\lambda_1\Delta t^2}[M](\{u^{t_p-1}\} + \Delta t\{\dot{u}^{t_p-1}\} + (0.5-\lambda_1)\Delta t^2\{\ddot{u}^{t_p-1}\}) \tag{61}$$

Using following equations the matrices of $[u^{t_p}]$, $[\dot{u}^{t_p}]$, and $[\ddot{u}^{t_p}]$ can be computed

$$\{u^{t_p}\} = [K_m]^{-1}\left\{f_m^{t_p}\right\} \tag{62}$$

$$\{\ddot{u}^{t_p}\} = \frac{1}{\lambda_1\Delta t^2}(\{u^{t_p}\} - \{u^{t_p-1}\} - \Delta t\{\dot{u}^{t_p-1}\} - \Delta t^2(0.5-\lambda_1)\{\ddot{u}^{t_p-1}\}) \tag{63}$$

$$\{\dot{u}^{t_p}\} = \{\dot{u}^{t_p-1}\} + \Delta t[(1-\lambda_2)\{\ddot{u}^{t_p-1}\} + \lambda_2\{\ddot{u}^{t_p}\}] \tag{64}$$

Using aforementioned equations, the matrices of $\{u^{t_p}\}$, $\{\dot{u}^{t_p}\}$, and $\{\ddot{u}^{t_p}\}$ can be obtained for an arbitrary time. The best convergence rate can be achieved in this method by choosing $\lambda_1 = 1/4$ and $\lambda_2 = 1/2$.

5. Verification

In this section, to demonstrate the capability and accuracy of the present method for dynamic analysis of the nanocomposite cylindrical shell, in the following, at first a problem is verified with analytical solution (Ugural and Fenster 2003) and then a cylindrical shell with the same geometry and boundary conditions (Shakeri *et al*. 2006) is solved using the present method and the results obtained for this analysis are compared. Shakeri *et al*. (2006) studied dynamic analysis of cylindrical shell using the FEM. Finally, the present method verified the results with those reported in the analysis done by Moradi-Dastjerdi *et al*. (2013) that in this analysis governing equations of nanocomposite cylindrical were solved using the element free Galerkin (EFG) method.

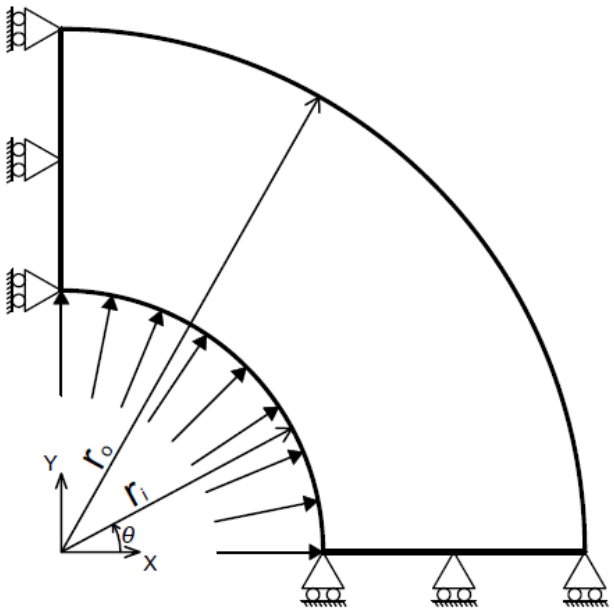

Fig. 5 The geometry and the boundary conditions

5.1 Verification with analytical solution

In this section, a cylindrical shell is considered with $r_i = 0.25\,m$, $r_o = 0.5\,m$, and, $\theta = {}^{\pi}/_{2}\ rad$, as the inner, outer radius, and angle of cylinder, respectively. The geometry and boundary conditions of this cylinder are showed in Fig. 5. The following boundary conditions are assumed for the problem to continue the study

$$\sigma_r\left(r_i,\theta,t\right)=P\left(t\right) \qquad \sigma_r\left(r_o,\theta,t\right)=0$$

$$\sigma_\theta\left(r_i,\theta,t\right)=0 \qquad \sigma_\theta\left(r_o,\theta,t\right)=0$$

$$\tau_{r\theta}\left(r_i,\theta,t\right)=0 \qquad \tau_{r\theta}\left(r_o,\theta,t\right)=0 \tag{65}$$

$$u_r\left(r,\theta_{min},t_0\right)=0 \qquad u_r\left(r,\theta_{max},t_0\right)=0$$

$$u_\theta\left(r,\theta_{min},t\right)=0 \qquad u_\theta\left(r,\theta_{max},t\right)=0$$

$$P\left(t\right)=P_0\left(1-e^{-c_0 t}\right) \tag{66}$$

where $P_0 = 20\ MPa$ and $c_0 = 10^2\ \frac{1}{sec}$ are assumed.

The results obtained for the cylindrical shell using analytical solution (Ugural and Fenster 2003) are as follow:

$$\sigma_{rr}=\frac{r_{in}^2 r_{out}^2\left(P_{out}-P_{in}\right)}{r_{out}^2-r_{in}^2}\frac{1}{r^2}+\frac{r_{in}^2 P_{in}-r_{out}^2 P_{out}}{r_{out}^2-r_{in}^2} \tag{67}$$

$$\sigma_{\theta\theta}=-\frac{r_{in}^2 r_{out}^2\left(P_{out}-P_{in}\right)}{r_{out}^2-r_{in}^2}\frac{1}{r^2}+\frac{r_{in}^2 P_{in}-r_{out}^2 P_{out}}{r_{out}^2-r_{in}^2} \tag{68}$$

$$u_{rr}=\frac{1+\nu}{E}\left[\begin{array}{l}\dfrac{r_{in}^2 r_{out}^2\left(P_{out}-P_{in}\right)}{r_{out}^2-r_{in}^2}\dfrac{1}{r}\\ +\left(1-2\nu\right)\dfrac{r_{in}^2 P_{in}-r_{out}^2 P_{out}}{r_{out}^2-r_{in}^2}r\end{array}\right] \tag{69}$$

also the terms $E_r = E_\theta = 70$ GPa and $\nu_{r\theta} = \nu_{\theta r} = 0.3$ are selected for the problem. It is possible the obtained results with those gotten from Eqs. (67)-(69) are compared. Fig. 6, shows the radial displacement through the thickness of the cylindrical shell. From this Figure can be seen a good agreement between results obtained from the present method with analytical solution. Figs. 7 and 8 depict the radial and hoop stress, respectively. From these Figures can be concluded the present method has high accuracy and capability to dynamic analysis of the cylindrical shell.

In Table 2 percentage errors for local Petrov–Galerkin method and the analytical solution in middle point of thickness of the cylinder (r=0.375 m) are shown. Table 2 indicates the relation done with local Petrov–Galerkin method has very high accuracy, thus this method can be used as a practical approach for dynamic analysis of cylindrical shell.

5.2 Verification with the finite element method (FEM)

Using the present work, we assume the nanocomposite cylindrical shell under shock loading with the same geometry and boundary conditions as the study of Shakeri *et al*. (2006), also boundary conditions can be found in Eq. (65). The cylinder is under shock loading as follows:

$$P\left(t\right)=\begin{cases}P_0 t & t\le t_0\\ 0 & t>t_0\end{cases} \tag{70}$$

where $P_0 = 4\ GPa/sec$ and $t_0 = 0.005\ sec$. Figs. 9-11 show a good agreement in comparison with results obtained by presented method and those reported in the study by Shakeri *et al*. (2006). This example proves the high capability and accuracy of this method to dynamic analysis of cylindrical shell.

In Table 3 the achieved results of local Petrov–Galerkin method with those got the finite element method (FEM) (Shakeri, Akhlaghi and Hosseini 2006) in middle point of thickness of the cylinder (r=0.375 m) are compared.

5.3 Verification with the element free Galerkin (EFG) method

In the following simulations a CNTRC cylinder made of Polymethyl-methacrylate (PMMA) as matrix, with CNT as fibers aligned in the axial direction is considered. PMMA is an isotropic material with $E^m = 2.5\,GPa$, $\rho^m = 1150\ kg/m^3$ and $\nu^m = 0.34$. The (10,10) single-walled carbon nanotubes (SWCNTs) are selected as reinforcements.

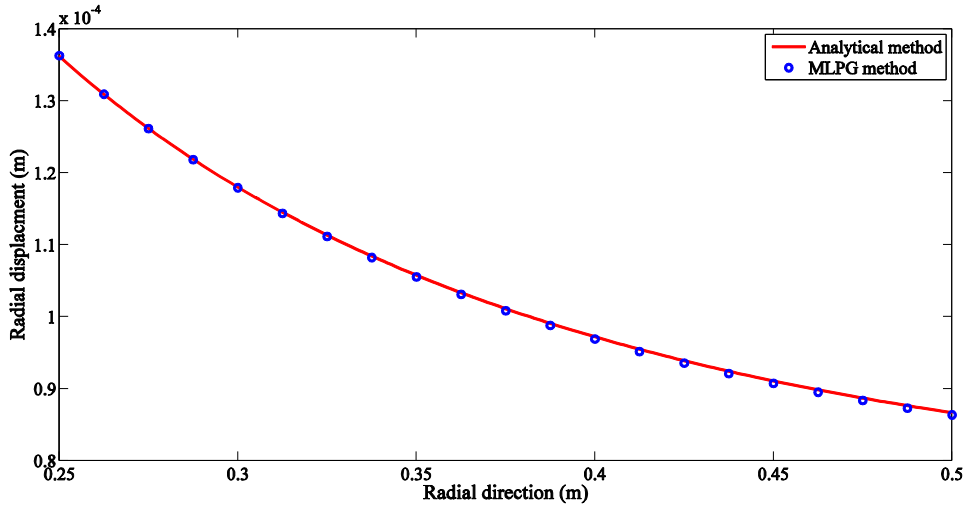

Fig. 6 The comparison of obtained results through the MLPG method with those gotten using analytical method for radial displacement

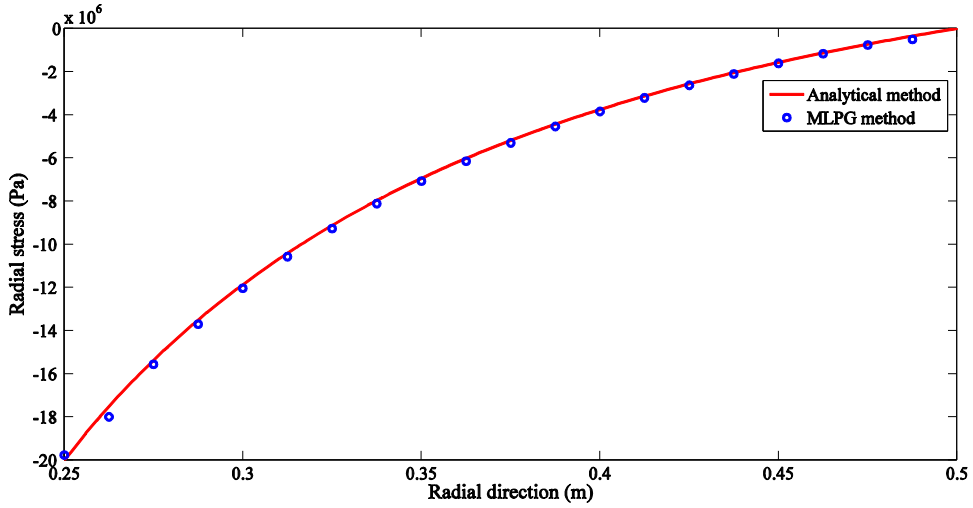

Fig. 7 The comparison of obtained results through the MLPG method with those gotten using analytical method for radial stress

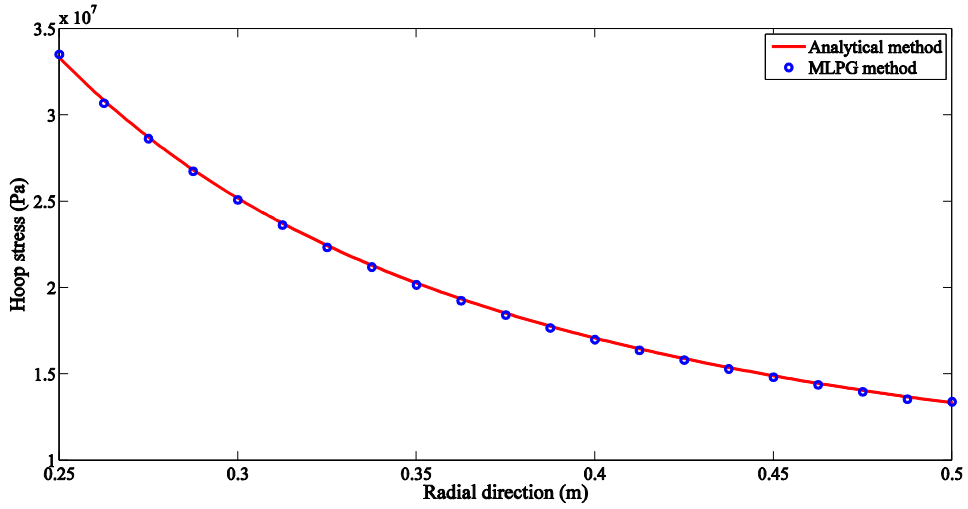

Fig. 8 The comparison of obtained results through the MLPG method with those gotten using analytical method for hoop stress

Table 2 The comparison of obtained results from the meshless local Petrov-Galerkin method with those gotten the analytical method for middle point of thickness of the cylinder

Variable	Analytical method (Ugural and Fenster 2003)	Local Petrov-Galerkin method	Percentage error
Displacement (m)	1.0111×10^{-4}	1.0112×10^{-4}	9.89×10^{-3}
Radial stress (Pa)	-5.185×10^{6}	-5.139×10^{6}	0.8872
Hoop stress (Pa)	1.852×10^{7}	1.842×10^{7}	0.5399

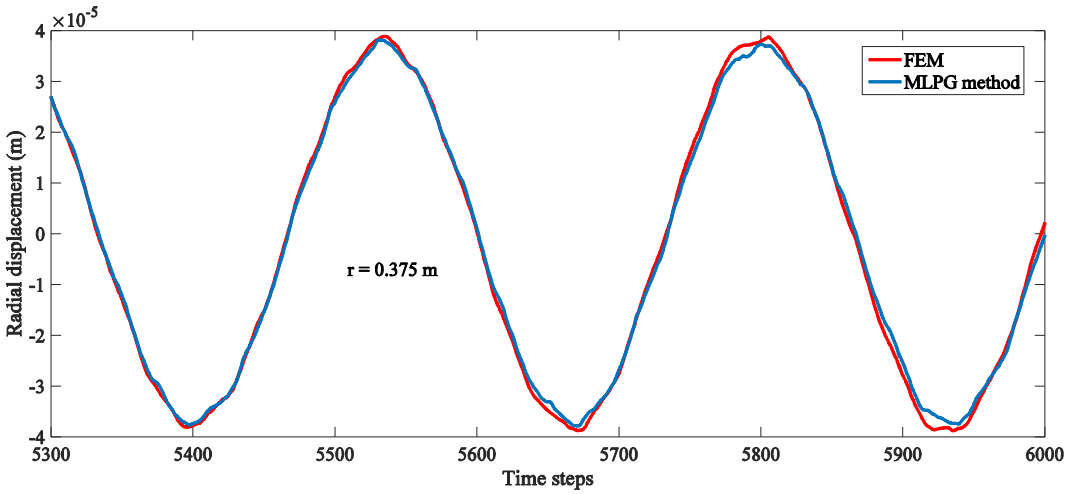

Fig. 9 The comparison of obtained results through the MLPG method with those gotten using FEM for radial displacement

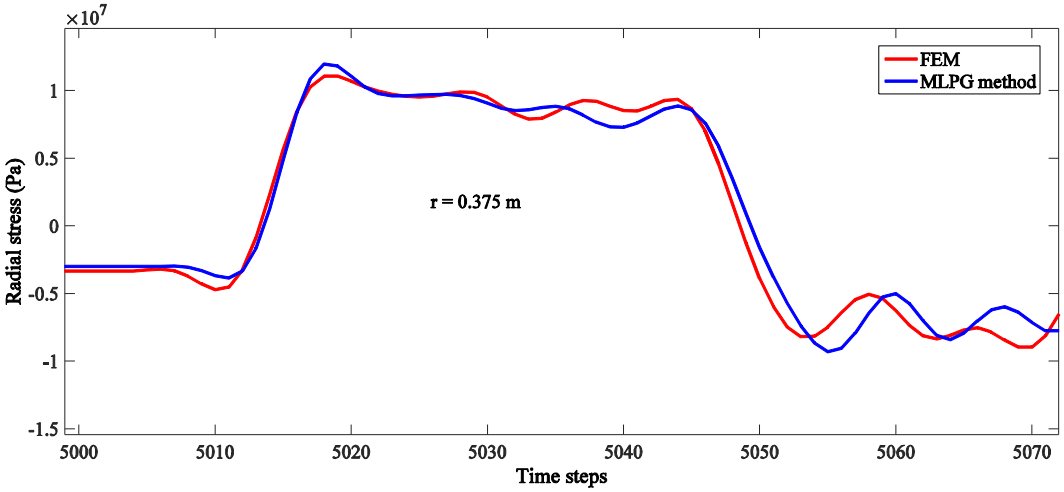

Fig. 10 The comparison of obtained results through the MLPG method with those gotten using FEM for radial stress

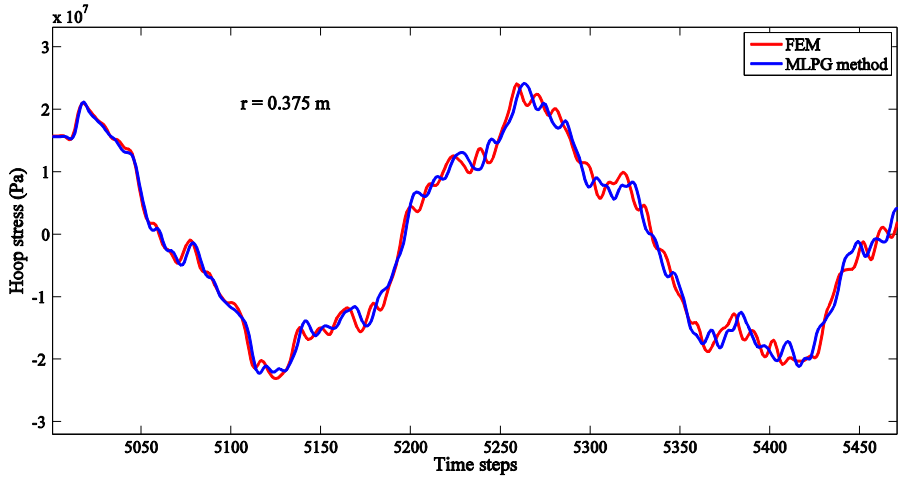

Fig. 11 The comparison of obtained results through the MLPG method with those gotten using FEM for hoop stress

Table 3 The comparison of obtained results from the meshless local Petrov-Galerkin method with those gotten the FEM for middle point of thickness of the cylinder

Variable	FEM (Shakeri, Akhlaghi and Hosseini 2006)	Local Petrov-Galerkin method	Percentage difference
Displacement (m)	-3.465×10^{-5}	-3.466×10^{-5}	0.011
Radial stress (Pa)	-9.885×10^{6}	-9.779×10^{6}	1.072
Hoop stress (Pa)	-2.441×10^{7}	-2.421×10^{7}	0.819

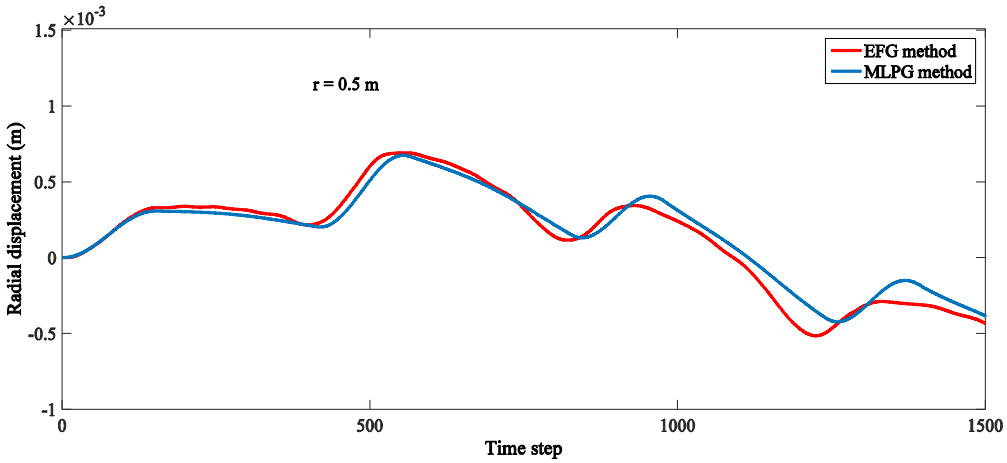

Fig. 12 The comparison of obtained results through the MLPG method with those gotten using EFG method for radial displacement

The material properties adopted for SWCNT are: $E_1^{CNT} = 5.6466\,TPa$, $E_2^{CNT} = 7.0800\,TPa$, $G_{12}^{CNT} = 1.9445\,TPa$, $\rho^{CNT} = 1400\,kg/m^3$ and $v_{12}^{CNT} = 0.175$ (Shen and Postbuckling 2011). Consider carbon nanotube-reinforced composite (CNTRC) cylinder with internal radius, $r_i = 0.5\,m$ and external radius, $r_o = 1\,m$ and use FG-X type of CNTRC cylinder with $V_{CNT}^{*} = 0.17$. This cylinder is subjected to an internal pressure expressed by

$$P(t) = P_0 sin\left(\frac{\pi t}{0.00015}\right) \qquad for\ t \le 0.00015\ s$$
$$P(t) = 0 \qquad for\ t > 0.00015\ s \tag{71}$$

where $P_0 = 10\,MPa$. Fig. 12 shows a good agreement in comparison to results obtained by the presented method and those reported in the scholarism of Shen and Postbuckling (2011). From these Figures can be concluded the present method has high accuracy and capability to dynamic analysis of the cylindrical shell.

6. Numerical example

In this section, we analyze the cylindrical shell made of nanocomposite material with four kinds of grading patterns and angle of nanocomposite reinforcements under shock loading with the meshless method. A non-symmetric nanocomposite cylinder is assumed, in which $r_i = 0.5\,m$, $r_o = 0.75\,m$, $\theta_{min} = 0\,rad$ and $\theta_{max} = \pi/2\,rad$ are considered as the inner and outer radius, minimum and maximum angle of cylinder, respectively (see Fig. 5). The boundary conditions are as follow:

$$\begin{aligned}
&\sigma_r(r_i,\theta,t) = P(t) && \sigma_r(r_o,\theta,t) = 0\\
&\sigma_\theta(r_i,\theta,t) = 0 && \sigma_\theta(r_o,\theta,t) = 0\\
&\tau_{r\theta}(r_i,\theta,t) = 0 && \tau_{r\theta}(r_o,\theta,t) = 0\\
&u_r(r,\theta_{min},t) = 0 && u_r(r,\theta_{max},t) = 0\\
&u_\theta(r,\theta_{min},t) = 0 && u_\theta(r,\theta_{max},t) = 0
\end{aligned} \tag{72}$$

$$P(t) = \begin{cases} P_0 & t \le 0.0002\ \text{sec} \quad 0 \le \theta \le \dfrac{\pi}{4} \\ 0 & t > 0.0002\ \text{sec} \quad \theta > \dfrac{\pi}{4} \end{cases} \tag{73}$$

where $P_0 = 5$ MPa is presumed. The mechanical features of this cylinder are shown in Table 4. Figs. 13-18 show the radial and hoop displacement for the various kinds of grading patterns and angle of nanocomposite reinforcements in the middle point of thickness of the cylinder $(r = 0.625\,m)$. Tables 5-6 show percentage of difference between displacements obtained from type UD of grading pattern with those gotten from other type of grading pattern. From Table 5 can be concluded the most percent difference occurs for type X of grading pattern and the lowest percentage difference is related to type V of grading pattern. Accordingly, Table 6 results the most percent difference is related to type X of grading pattern and the lowest percentage difference occurs for type Λ of grading pattern.

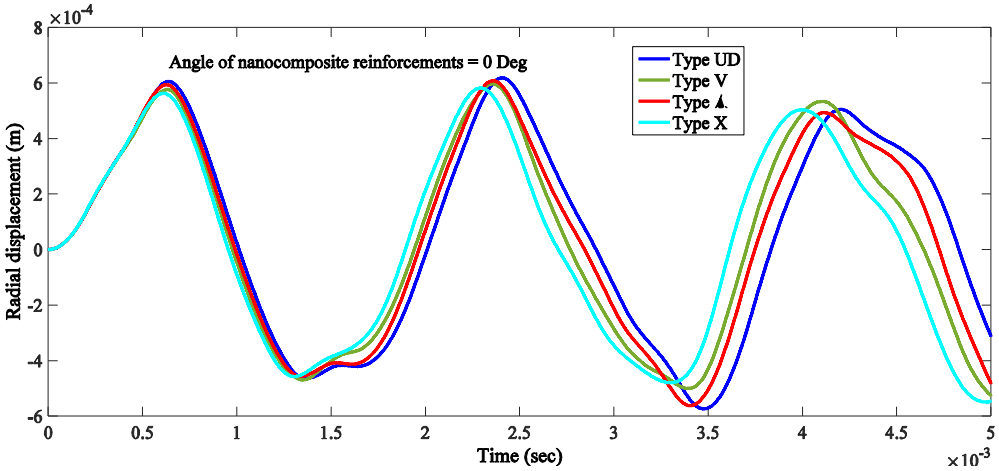

Fig. 13 The radial displacements for the various kinds of grading patterns in the middle point of thickness of the cylinder $(r = 0.625\ m)$ and angle of nanocomposite reinforcements =0 Deg

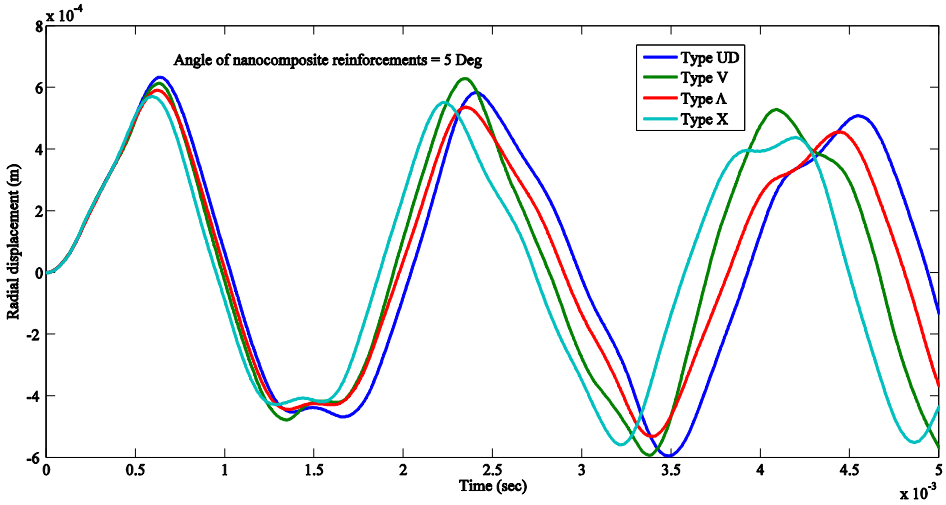

Fig. 14 The radial displacements for the various kinds of grading patterns in the middle point of thickness of the cylinder $(r = 0.625\ m)$ and angle of nanocomposite reinforcements =5 Deg

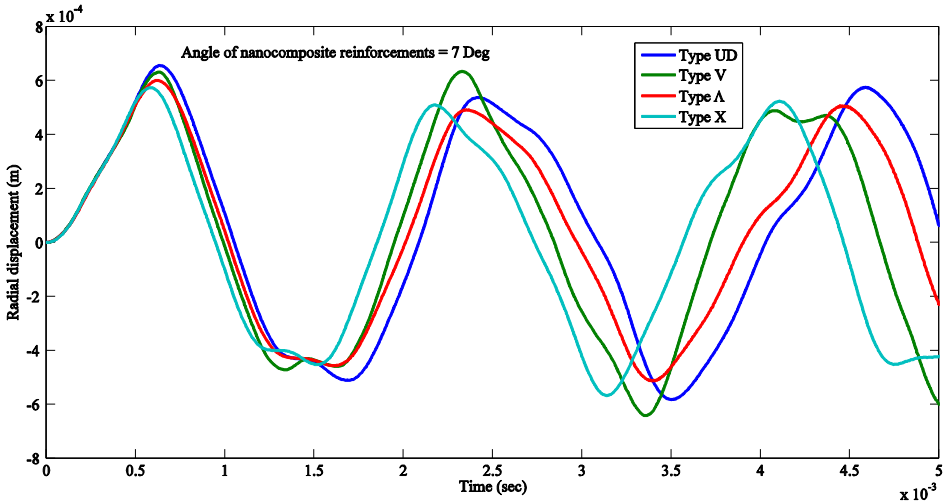

Fig. 15 The radial displacements for the various kinds of grading patterns in the middle point of thickness of the cylinder $(r = 0.625\ m)$ and angle of nanocomposite reinforcements =7 Deg

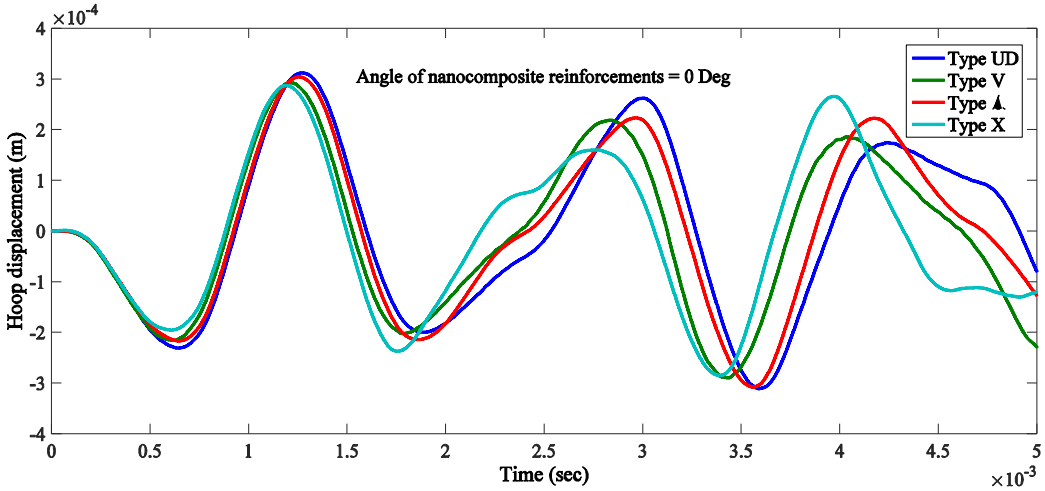

Fig. 16 The hoop displacements for the various kinds of grading patterns in the middle point of thickness of the cylinder $(r = 0.625\ m)$ and angle of nanocomposite reinforcements =0 Deg

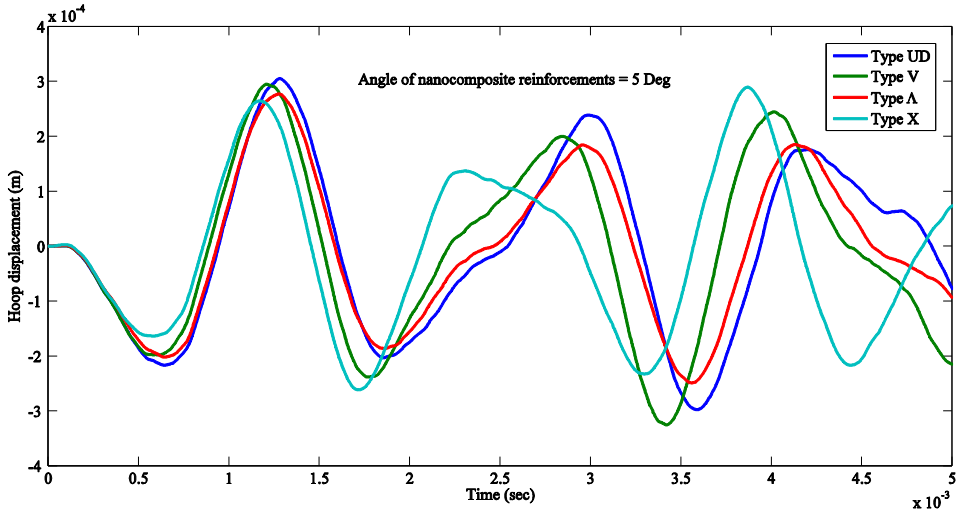

Fig. 17 The hoop displacements for the various kinds of grading patterns in the middle point of thickness of the cylinder $(r = 0.625\ m)$ and angle of nanocomposite reinforcements =5 Deg

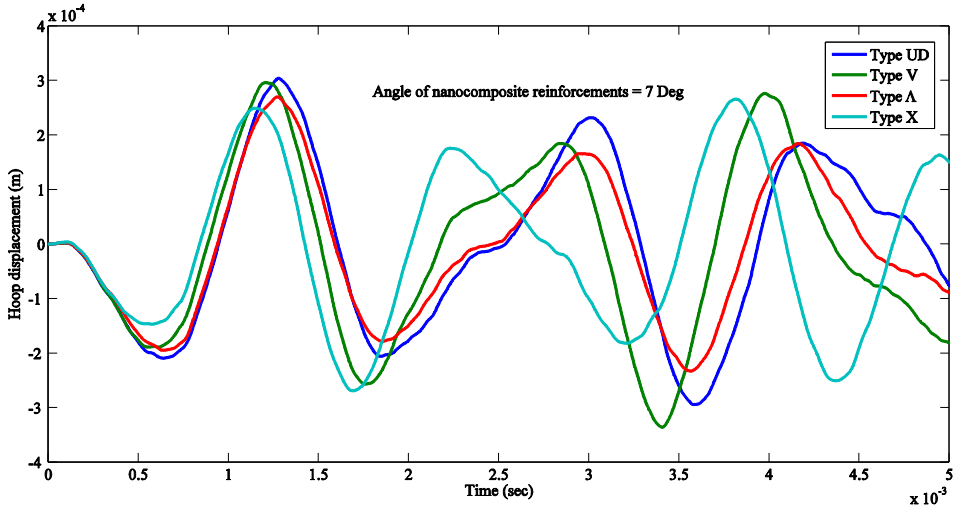

Fig. 18 The hoop displacements for the various kinds of grading patterns in the middle point of thickness of the cylinder $(r = 0.625\ m)$ and angle of nanocomposite reinforcements =7 Deg

Table 4 Comparisons of Youngs moduli for polymer/CNT composites reinforced by (10, 10) SWCNT at $T_0 = 300\,K$ (Shen and Zhang 2010)

V^*_{CNT}	MD (Han and Elliott 2007)		Extended rule of mixture			
	$E_{11}(GPa)$	$E_{22}(GPa)$	$E_{11}(GPa)$	η_1	$E_{22}(GPa)$	η_2
0.12	94.6	2.9	94.78	0.137	2.9	1.022
0.17	138.9	4.9	138.68	0.142	4.9	1.626
0.28	224.2	5.5	224.5	0.141	5.5	1.585

Table 5 The difference percentage of radial displacement for type UD of grading patterns with other types of grading patterns

Type	fiber angle		
	0	**5**	**7**
Type V	3.37	0.73	3.51
Type Λ	1.71	6.9	8.46
Type X	3.98	10.41	12.62

Table 6 The difference percentage of hoop displacement for type UD of grading patterns with other types of grading patterns

Type	fiber angle		
	0	**5**	**7**
Type V	6.42	3.44	2.57
Type Λ	2.4	9.23	11.12
Type X	7.92	5.17	12.57

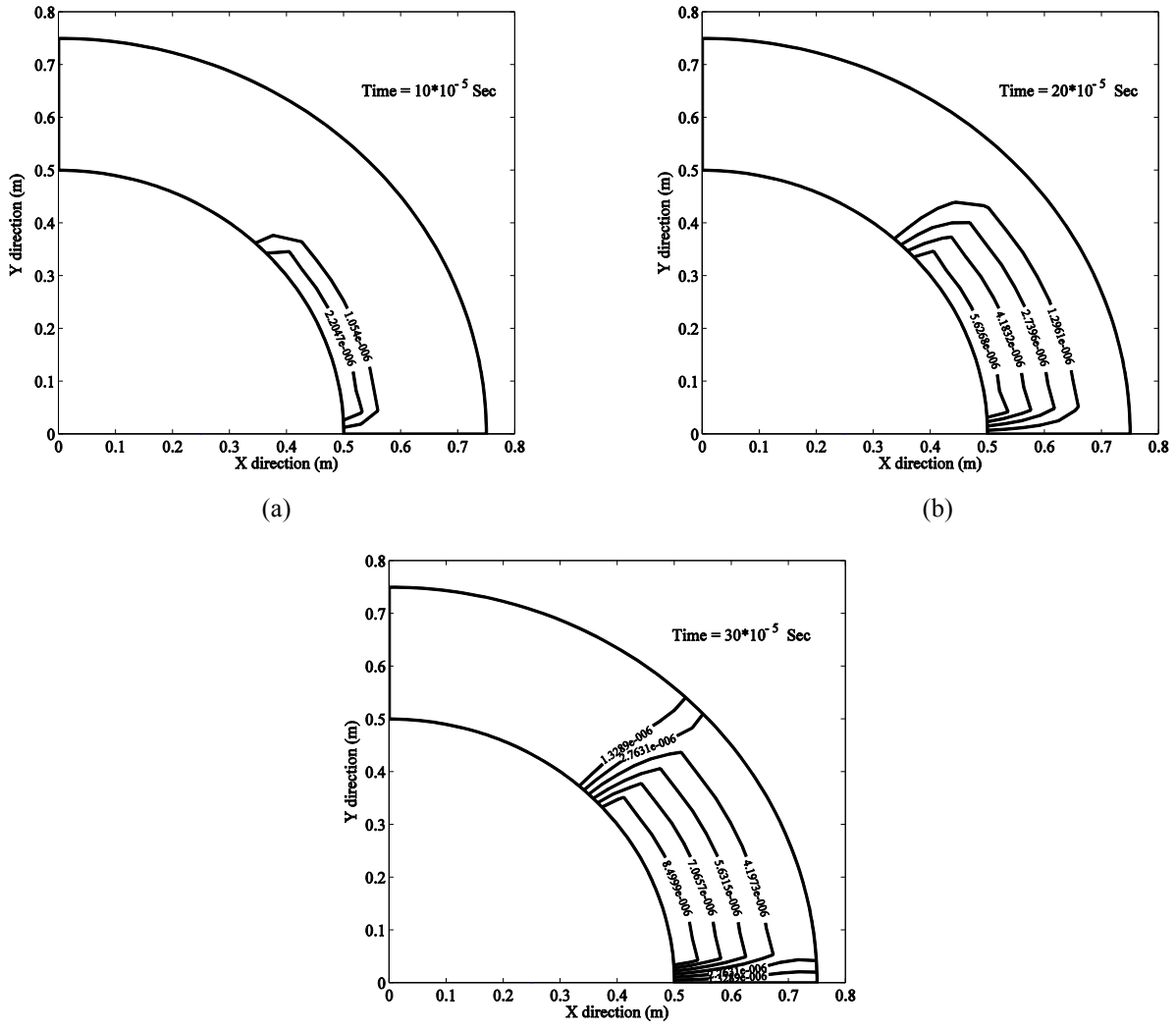

(a) (b)

(c)

Fig. 19 Wave propagation for radial displacement and type UD of grading patterns which angle of nanocomposite reinforcements = 0 Deg

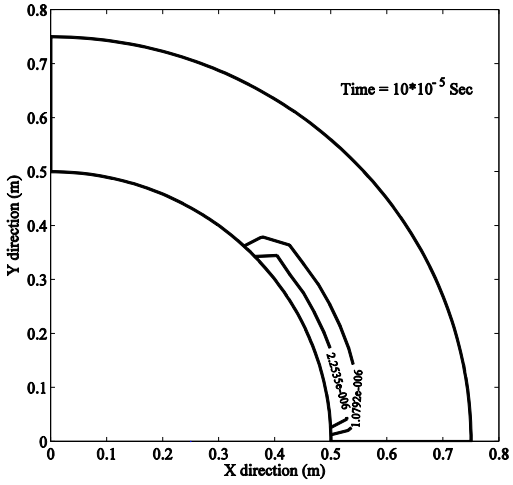

(a)

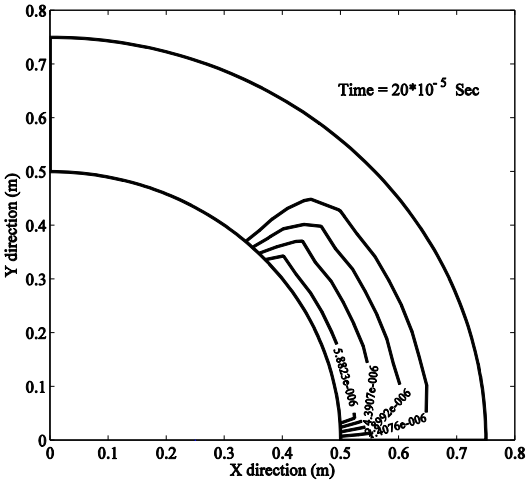

(b)

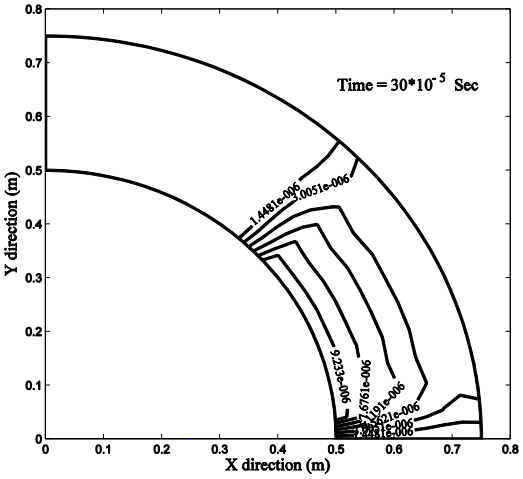

(c)

Fig. 20 Wave propagation for radial displacement and type UD of grading patterns which angle of nanocomposite reinforcements = 5 Deg

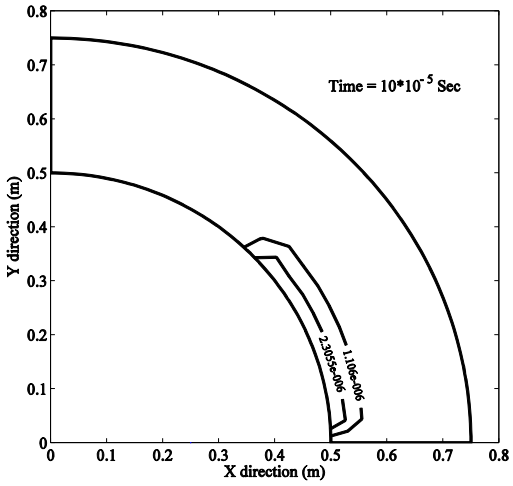

(a)

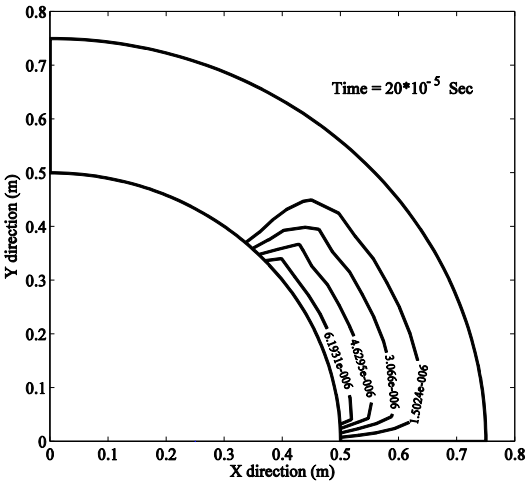

(b)

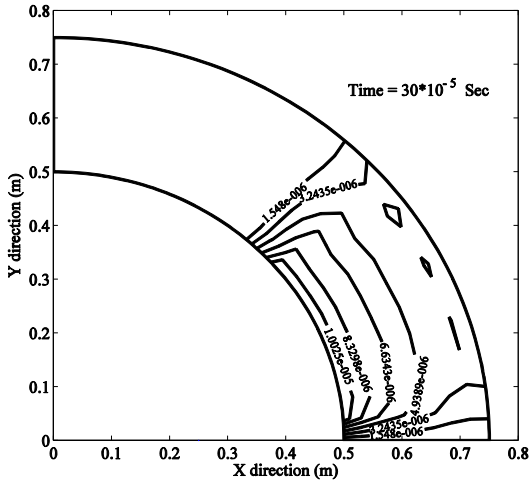

(c)

Fig. 21 Wave propagation for radial displacement and type UD of grading patterns which angle of nanocomposite reinforcements = 7 Deg

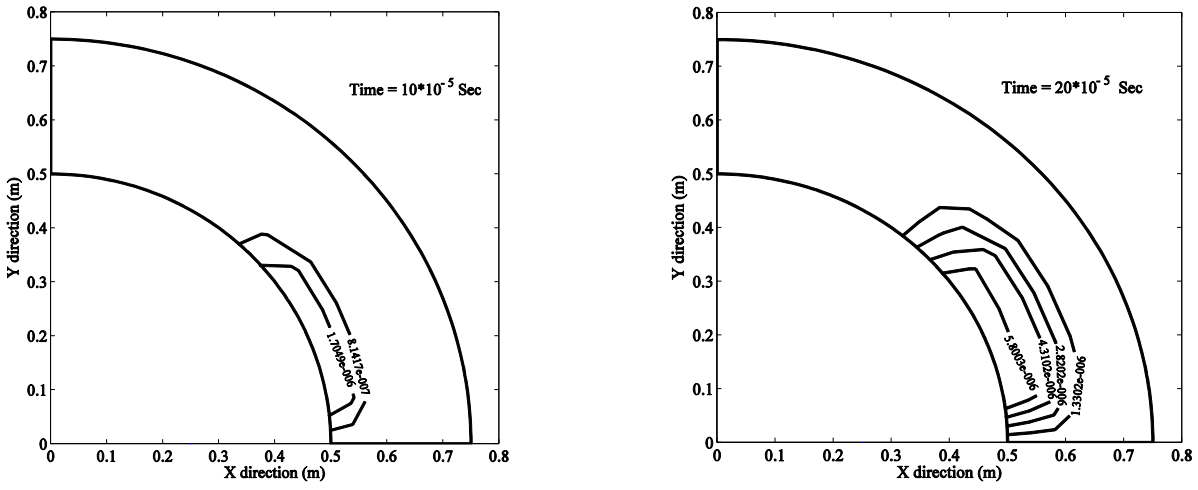

(a) (b)

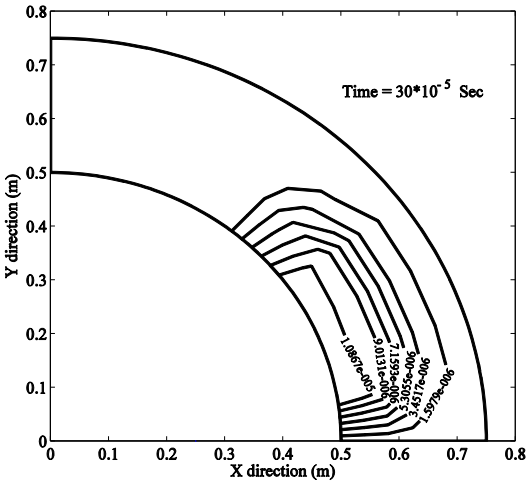

(c)

Fig. 22 Wave propagation for radial displacement and type X of grading patterns which angle of nanocomposite reinforcements = 0 Deg

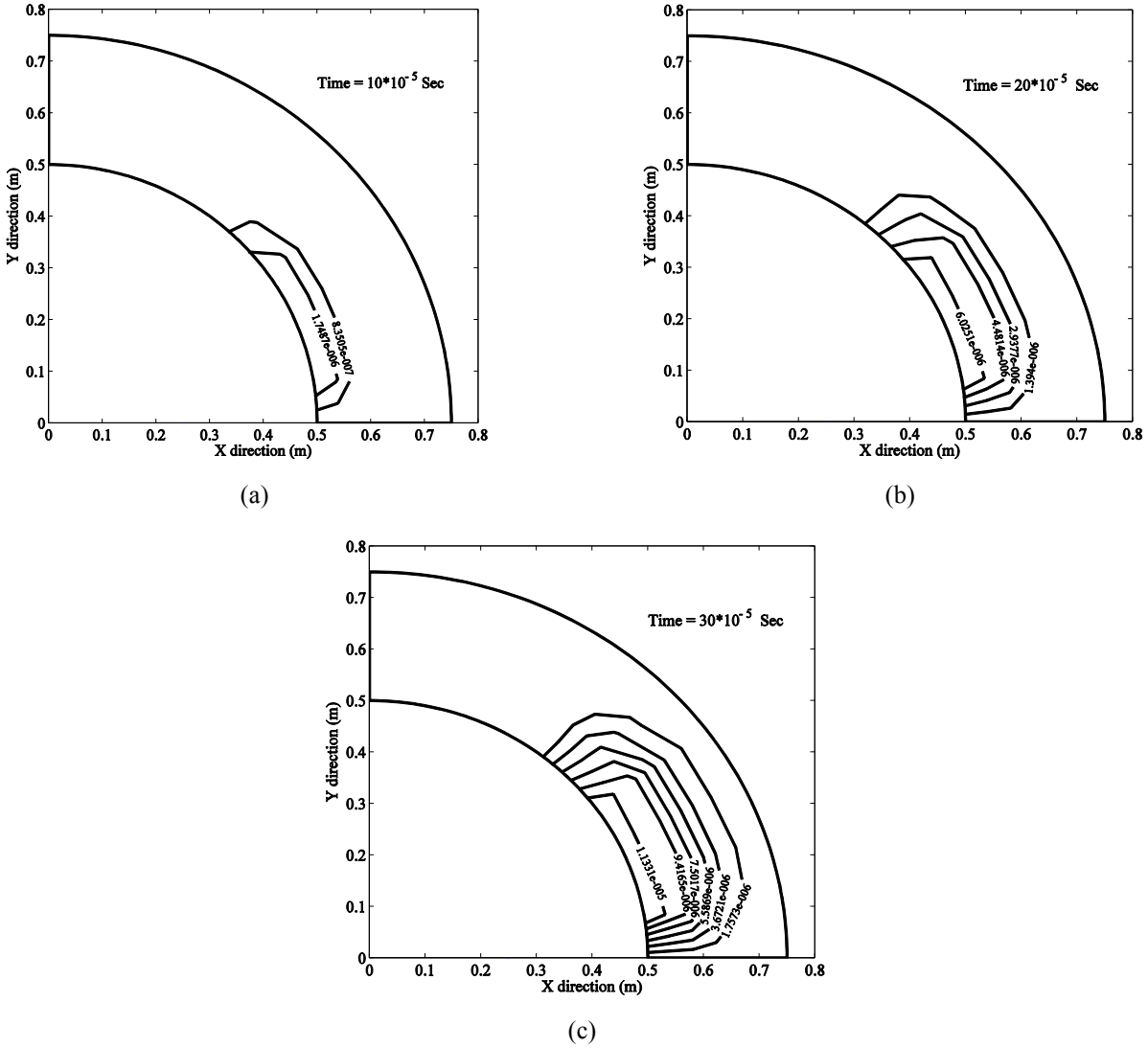

Fig. 23 Wave propagation for radial displacement and type X of grading patterns which angle of nanocomposite reinforcements = 5 Deg

Figs. 19-24 show radial displacement wave propagation for type UD and the fourth of grading pattern with various angle of nanocomposite reinforcements. From these Figures can be concluded for type UD and the fourth of grading pattern with increasing of the angle of nanocomposite reinforcements, the radial displacement increases. By comparison the wave propagation of two kinds of grading patterns can be shown the velocity of wave propagation for type UD is more than of type X.

7. Conclusion

The MLPG method is used to analyze non-symmetric nanocomposite cylinder reinforced by different angle of carbon nanotubes reinforcement. The micro mechanical model is applied to mechanical properties of the nanocomposite cylinder. The Newmark time approximation scheme with suitable time step was employed for transfer the derived equation with MLPG method in time domain. The brief outline that it has been obtained through the above analysis is as follows:

- The non-symmetric nanocomposite cylinder under shock loading is analyzed based on meshless local Petrov-Galerkin (MLPG) method.
- A comparison between the obtained results from the present method with analytical method demonstrates the accuracy and effectiveness of the presented MLPG method for analyze non-symmetric nanocomposite cylinder.
- To show capacity of the present method for shock loading analysis, this method compares with FEM and EFG method. The accuracy and the convergence of the presented method for shock loading analysis have been demonstrated.
- From analyses of the non-symmetric

nanocomposite cylindrical shell can be concluded for radial displacement, the most percent difference occurs for type X of grading pattern and the lowest percentage difference is related to type V of grading pattern.

- By comparing the aligned fibers for hoop displacement can be resulted the most percent difference is related to type X of grading pattern and the lowest percentage difference occurs for type Λ of grading pattern.
- By increasing the angle of nanocomposite reinforcements, the values of radial displacement contours are increased and the wave propagation speed is increased.
- By comparison the wave propagation of two kinds of grading pattern can be shown the velocity of wave propagation for type UD is more than type X.

The present analysis furnishes a ground for dynamic analyses and wave propagation of non-symmetric nanocomposite cylindrical shell with various kinds of grading patterns and angle of nanocomposite reinforcements under shock loading.

References

Alibeigloo, A. (2016), "Elasticity solution of functionally graded carbon nanotube-reinforced composite cylindrical panel subjected to thermo mechanical load", *Compos. Part B Eng.*, **87**, 214-226. https://doi.org/10.1016/j.compositesb.2015.09.060.

Ansari, R., Faghih Shojaei, M., Mohammadi, V., Gholami, R. and Sadeghi, F. (2014), "Nonlinear forced vibration analysis of functionally graded carbon nanotube-reinforced composite Timoshenko beams", *Compos. Struct.*, **113**, 316–327. https://doi.org/10.1016/j.compstruct.2014.03.015

Atluri, S.N. and Zhu, T. (1998), "A New Meshless Local Petrov–Galerkin (MLPG) Approach in Computational Mechanics", *Comput. Mech.*, **22**(2), 117–127. https://doi.org/10.1007/s004660050346.

Bafekrpour, E., Yang, C., Natali, M. and Fox, B. (2013), "Functionally graded carbon nanofiber/phenolic nanocomposites and their mechanical properties", *Compos. Part B Appl. Sci. Manufact.*, **54**, 124–134. https://doi.org/10.1016/j.compositesa.2013.07.009.

Baltacıoglu, A.K., Akgoz, B. and Civalek, O. (2010), "Nonlinear static response of laminated composite plates by discrete singular convolution method", *Compos. Struct.*, **93**, 153–161. https://doi.org/10.1016/j.compstruct.2010.06.005.

Baltacıoglu, A.K., Civalek, O., Akgoz, B. and Demir, F. (2011), "Large deflection analysis of laminated composite plates resting on nonlinear elastic foundations by the method of discrete singular convolution", *J. Pressure Vessels Piping*, **88**, 290-300. https://doi.org/10.1016/j.ijpvp.2011.06.004.

Bian, Z.G. and Wang, Y.H. (2013), "Axisymmetrical bending of single- and multi-span functionally graded hollow cylinders", *Struct. Eng. Mech.*, **45**(3), 355-371. https://doi.org/10.12989/sem.2013.45.3.355.

Civalek, O. (2006), "The determination of frequencies of laminated conical shells via the discrete singular convolution method", *J. Mech. Mater. Struct.*, **1**, 163-182. http://dx.doi.org/10.2140/jomms.2006.1.163.

Civalek, O. (2008), "Analysis of thick rectangular plates with symmetric cross-ply laminates based on first-order shear deformation theory", *J. Compos. Mater.*, **42**(26), 2853-2867. https://doi.org/10.1177/0021998308096952.

Civalek, O., Korkmaz, A. and Demir, C. (2010), "Discrete singular convolution approach for buckling analysis of rectangular Kirchhoff plates subjected to compressive loads on two-opposite edges", *Adv. Eng. Software*, **41**(4), 557-560. https://doi.org/10.1016/j.advengsoft.2009.11.002.

Coto, B., Antia, I., Blanco, M., Martinez-de-Arenaza, I., Meaurio, E., Barriga, J. and Sarasua, J.R. (2011), "Molecular dynamics study of the influence of functionalization on the elastic properties of single and multiwall carbon nanotubes", *Comput. Mater. Sci.*, **50**(12), 3417–3424. https://doi.org/10.1016/j.commatsci.2011.07.003.

Ghadiri Rad, M.H., Shahabian, F. and Hosseini, S.M. (2015), "Geometrically nonlinear elastodynamic analysis of hyper-elastic neo-Hooken FG cylinder subjected to shock loading using MLPG method", *Eng. Analysis Boundary Elements*, **50**, 83–96. https://doi.org/10.1016/j.enganabound.2014.08.002.

Ghannad, M., Zamani Nejad, M., Rahimi, G.H. and Sabouri, H. (2012), "Elastic analysis of pressurized thick truncated conical shells made of functionally graded materials", *Struct. Eng. Mech.*, **43**(1), 105-126. https://doi.org/10.12989/sem.2012.43.1.105.

Ghayoumizadeh, H., Shahabian, F. and Hosseini, S.M. (2013), "Elastic wave propagation in a functionally graded nanocomposite reinforced by carbon nanotubes employing meshless local integral equations (LIEs)", *Eng. Analysis Boundary Elements*, **37**(11), 1524–1531. https://doi.org/10.1016/j.enganabound.2013.08.011.

Gürses, M., Civalek, O., Korkmaz, A. and Ersoy, H. (2009), "Free vibration analysis of symmetric laminated skew plates by discrete singular convolution technique based on first-order shear deformation theory", *J. Numeric Methods Eng.*, **79**(3), 290-313. https://doi.org/10.1002/nme.2553.

Han, Y. and Elliott, J. (2007), "Molecular dynamics simulations of the elastic properties of polymer/carbon nanotube composites", *Comput. Mater. Sci.*, **39**(2), 315–323. https://doi.org/10.1016/j.commatsci.2006.06.011.

Heydarpour, Y., Aghdam, M.M. and Malekzadeh, P. (2014), "Free vibration analysis of rotating functionally graded carbon nanotube-reinforced composite truncated conical shells", *Compos. Struct.*, **117**, 187-200. https://doi.org/10.1016/j.compstruct.2014.06.023.

Hosseini, S.M. (2012), "Analysis of elastic wave propagation in a functionally graded thick hollow cylinder using a hybrid mesh-free method", *Eng. Analysis Boundary Elements*, **36**(11), 1536–1545. https://doi.org/10.1016/j.enganabound.2012.05.001.

Hosseini, S.M., Sladek, J. and Sladek, V. (2011), "Meshless local Petrov–Galerkin method for coupled thermoelasticity analysis of a functionally graded thick hollow cylinder", *Eng. Analysis Boundary Elements*, **35**(6), 827–835. https://doi.org/10.1016/j.enganabound.2011.02.001.

Jin, G., Te, Y., Me, X., Chen, Y., Su, X. and Xie, X. (2013), "A unified approach for the vibration analysis of moderately thick composite laminated cylindrical shells with arbitrary boundary conditions", *J. Mech. Sci.*, **75**, 357–376. https://doi.org/10.1016/j.ijmecsci.2013.08.003.

Lei, Z.X., Liew, K.M. and Yu, J.L. (2013), "Buckling analysis of functionally graded carbon nanotube-reinforced composite plates using the element-free kp-Ritz method", *Compos. Struct.*, **98**, 160–168. https://doi.org/10.1016/j.compstruct.2012.11.006.

Liaw, J.W. (2006), "Analysis of the surface plasmon resonance of a single core-shelled nanocomposite by surface integral equations", *Eng. Analysis Boundary Elements*, **30**(9), 734–745. https://doi.org/10.1016/j.enganabound.2006.03.009.

Liew, K.M., He, X.Q., Tan, M.J. and Lim, H.K. (2004), "Dynamic

analysis of laminated composite plates with piezoelectric sensor/actuator patches using the FSDT mesh-free method", *J. Mech. Sci.,* **46**, 411–431. https://doi.org/10.1016/j.ijmecsci.2004.03.011.

Moradi-Dastjerdi, R., Foroutan, M. and Pourasghar, A. (2013), "Dynamic analysis of functionally graded nanocomposite cylinders reinforced by carbon nanotube by a mesh-free method", *Mater. Design*, **44**, 256-266. https://doi.org/10.1016/j.matdes.2012.07.069.

Rezaei Mojdehi, A., Darvizeh, A., Basti, A. and Rajabi, H. (2011), "Three dimensional static and dynamic analysis of thick functionally graded plates by the meshless local Petrov–Galerkin (MLPG) method", *Eng. Analysis Boundary Elements*, **35**(11), 1168–1180. https://doi.org/10.1016/j.enganabound.2011.05.011.

Shakeri, M., Akhlaghi, M. and Hoseini, S.M. (2006), "Vibration and radial wave propagation velocity in functionally graded thick hollow cylinder", *Compos. Struct.*, **76**(1-2), 174–181. https://doi.org/10.1016/j.compstruct.2006.06.022.

Shen, H.S. (2011), "Postbuckling of nanotube–reinforced composite cylindrical shells in thermal environments, Part I: axially-loaded shells", *Compos. Struct.*, **93**(8), 2096-2108. https://doi.org/10.1016/j.compstruct.2011.02.011.

Shen, H.S. (2012), "Thermal buckling and postbuckling behavior of functionally graded carbon nanotube-reinforced composite cylindrical shells", *Compos. Part B Eng.*, **43**(3), 1030–1038. https://doi.org/10.1016/j.compositesb.2011.10.004.

Shen, H.S. and Zhang, C.L. (2010), "Thermal buckling and postbuckling behavior of functionally graded carbon nanotube–reinforced composite plates", *Mater. Design*, **31**(7), 3403–3411. https://doi.org/10.1016/j.matdes.2010.01.048.

Tadeu, A., Stanak, P., Antonio, J., Sladek, J. and Sladek, V. (2015), "2.5D elastic wave propagation in non-homogeneous media coupling the BEM and MLPG methods", *Eng. Analysis Boundary Elements*, **53**, 86–99. https://doi.org/10.1016/j.enganabound.2014.12.010.

Talebitooti, M. (2013), "Three-dimensional free vibration analysis of rotating laminated conical shells: layerwise differential quadrature (LW-DQ) method", *Arch. Appl. Mech.*, **83**, 765–781. https://doi.org/10.1007/s00419-012-0716-3.

Ugural, A.C. and Fenster, S.K. (2003), *Advanced Strength and Applied Elasticity*, (4th Edition), Prentice Hall, New York, NY, USA.

Wu, C.P. and Liu, Y.C. (2016), "A state space meshless method for the 3D analysis of FGM axisymmetric circular plates", *Steel and Compos. Struct.,* **22**(1), 161-182. https://doi.org/10.12989/scs.2016.22.1.161

Xiang, S. and Chen, Y. (2014), "meshless local collocation method for natural frequencies and mode shapes of laminated composite shells", *Struct. Eng. Mech.,* **51**(6), 893-907. https://doi.org/10.12989/sem.2014.51.6.893.

Xiang, Y., Ma, Y.F., Kitiornchai, S., Lim, C.W. and Lau, C.W.H. (2002), "Exact solutions for vibration of cylindrical shells with intermidiate ring supports", *J. Mech. Sci.*, **44**, 1907–1924. https://doi.org/10.1016/S0020-7403(02)00071-1.

Yas, M.H. and Heshmati M. (2012), "Dynamic analysis of functionally graded nanocomposite beams reinforced by randomly oriented carbon nanotube under the action of moving load", *Appl. Math. Modelling*, **36**(4), 1371–1394. https://doi.org/10.1016/j.apm.2011.08.037.

Ying, L.S., Mohd Salleh, M.A., Mohamed Yusoff, H.b., Abdul Rashid, S.B. and Abd Razak, J.b. (2011), "Continuous production of carbon nanotubes-A review", *J. Industrial Eng. Chem.*, **17**(3), 367–376. https://doi.org/10.1016/j.jiec.2011.05.007.

Zhang, L.W. (2017), "An element-free based IMLS-Ritz method for buckling analysis of nanocomposite plates of polygonal planform", *Eng. Analysis Boundary Elements*, **77**, 10–25. https://doi.org/10.1016/j.enganabound.2017.01.004.

Zhang, L.W., Xiao, L.N., Zou, G.L. and Liew, K.M. (2016), "Elastodynamic analysis of quadrilateral CNT-reinforced functionally graded composite plates using FSDT element-free method", *Compos. Struct.*, **148**, 144-154. https://doi.org/10.1016/j.compstruct.2016.04.006.

Zhu, R., Pan, E. and Roy, A.K. (2007), "Molecular dynamics study of the stress-strain behavior of carbon-nanotube reinforced Epon 862 composites", *Mater. Sci. Eng.*, **447**(1-2), 51–57. https://doi.org/10.1016/j.msea.2006.10.054.

PL